

HEAT FLOW IN LIQUID HELIUM
WITH CLAMPED NORMAL FLUID

Thesis by
Gerald Leslie Pollack

In Partial Fulfillment of the Requirements
For the Degree of
Doctor of Philosophy

California Institute of Technology
Pasadena, California

1962

ACKNOWLEDGEMENTS

These experiments were conceived by Professor John R. Pellam. I am much indebted to him for his guidance and encouragement and for many penetrating insights into related problems.

ABSTRACT

With very few additional assumptions the wave equations for First Sound and Second Sound in liquid helium admit of simultaneous solution for the motion of both superfluid and normal fluid in the presence of a large viscous force on the normal fluid. If these fluids are set in motion by the presence of heat energy their consequent motion, through a viscous medium, is a mixture of two modes - a diffusive heat flow and a wave heat flow. These experiments aim at seeking each of these modes and examining them. It was found that the only observable heat was transmitted diffusively although a very high degree of experimental sensitivity to waves was reached. The investigation includes heat transmission by both pulses and monochromatic waves and the viscous medium varies from coarse emery powder to very tightly packed rouge. The measurements were carried out at temperatures from 1.3°K to the lambda point. The consequences of the absence of waves are analyzed.

Table of Contents

<u>Part</u>		<u>Page</u>
	Introduction	1
I	Experimental Part	5
	I.1 The Pulse Method	5
	I.2 Results of the Pulse Method	10
	I.3 The Standing Wave Method	12
	I.4 Results of the Standing Wave Method	22
II	Theoretical Part	27
III	Conclusions	40
	References	43
	Figures	44

Figures

<u>Number</u>	<u>Title</u>	<u>Page</u>
1	Velocity of Second Sound in Helium Using Pulse Method	45
2	Apparent Velocity of Second Sound Through #46 Emery Powder	46
3	Apparent Velocity of Second Sound Through Grit #100 Emery Powder	47
4	Apparent Velocity of Second Sound Through Grit #150 Emery Powder	48
5	Apparent Velocity of Second Sound Through Grit #200 Emery Powder	49
6	Apparent Velocity of Second Sound Through Grit #320 Emery Powder	50
7	Apparent Velocity of Second Sound Through Grit #400 Emery Powder	51
8	Apparent Velocity of Second Sound Through Grit #600 Emery Powder	52
9	Apparent Velocity of Second Sound in Helium as Function of Rouge Density with Pulse Method	53
10	Apparent Velocity of Second Sound Through Zeolite	54
11	Schematic of Electronic System for Pulse Method	55
12	Schematic of Electronic System for Standing Wave Method	56
13A	Typical Receiver or Transmitter Element	57
13B	Typical Combined Receiver and Transmitter Element	57
14	Velocity of Second Sound in Helium Using Standing Waves	58
15	Velocity of Second Sound in Helium Using Standing Waves with Combined Receiver-Transmitter Element	59
16	Spectrum of Signal as Function of Frequency of Second Sound for Container 16.0% Filled with Rouge	60

Figures (continued)

<u>Number</u>	<u>Title</u>	<u>Page</u>
17	Spectrum of Signal as Function of Frequency of Second Sound for Container 16.4% Filled with Lucite . . .	61
18	Construction Detail of the Resonant Chamber with Variable Height . . .	62
19	Spectrum of Signal Height as Function of Reciprocal of Signal Generator Frequency All Measured at Several Chamber Heights with Rouge Bottom . . .	63
20	Spectrum of Signal Height as Function of Reciprocal of Signal Generator Frequency All Measured at Several Chamber Heights with Lucite Bottom . . .	64
21	Spectrum of Signal versus Reciprocal of Signal Generator Frequency with Spacer in Place T = 1.288°K . . .	65
22	Spectrum of Signal versus Reciprocal of Signal Generator Frequency with Spacer in Place T = 2.085°K . . .	66
23	Spectrum of Signal versus Reciprocal of Signal Generator Frequency with Spacer in Place T = 2.141°K . . .	67
24	Theoretical Velocity of New Thermal Waves as Function of Temperature . . .	68
25	Plot of $\left(\frac{v_1}{v}\right)^2$ versus $T^{-5/2}$ for Grit #100 Emery Powder . . .	69
26	Plot of $\left(\frac{v_1}{v}\right)^2$ versus $T^{-5/2}$ for Dense Rouge (1.03gm/cm ³) . . .	70

Introduction

The properties of liquid helium are qualitatively different from those of any other known liquid. It is because of this uniqueness that their investigation has been so avidly pursued since helium was first liquefied in 1908 by Kammerlingh-Onnes. There is no other substance which offers so much opportunity for understanding the liquid state.

The first real success in understanding came with the proposal by F. London (1) that since both the Van der Waal's forces between helium atoms and the density of the liquid are small, the liquid closely approximates an ideal gas. Since naturally occurring helium is overwhelmingly He^4 and since He^4 obeys symmetrical statistics, we have to deal with a Bose-Einstein gas. The theory of such a gas exhibits a critical temperature, a discontinuous derivative in the specific heat at this temperature, and other properties rather similar to those actually observed in liquid helium. This idea was further developed by Tisza (2), who associated the atoms which fall into the ground state below the critical temperature (λ point) with a "superfluid" and the excited atoms with a "normal fluid." The superfluid atoms were supposed to be able to flow through even the smallest orifices with no viscosity because they could not lose any energy to their surroundings. Shortly after this Tisza (3) used this two fluid model of liquid helium

to predict the existence of thermal waves below the lambda point (approximately 2.19°K). Landau (4) found fault with Tisza's theory by noticing that although the ground state atoms could not lose energy to their surroundings, they might gain energy and thus be raised to the normal state with attendant viscosity. Nevertheless, the essentials of the two-fluid model were retained by introducing an operator formalism for quantizing the liquid and independently deriving an expression for the velocity of thermal waves from hydrodynamical equations of motion.

These thermal waves, which have since come to be called "second sound," were first observed by Peshkov (5, 6) using a standing wave method, and were more exhaustively studied by Pellam (7, 8), using a pulse method, so that their velocity is well known and their nature well understood. According to the two-fluid model, a local increase in temperature below the lambda point is associated with a dearth of ground state atoms and a local decrease in temperature is associated with an excess of them. The transport of a temperature front is then merely an interflow of superfluid atoms toward the heat source and of normal atoms away from it in such a way that the net momentum is zero. A thermal wave of frequency f say, traveling through the liquid, sets these two fluids to interflowing as above, but this time with frequency f , and again with zero net momentum.

The properties of liquid helium in transmitting density waves, i. e., ordinary or first sound, are less anomalous but likewise essential to our purposes. Their velocity was variously measured using a standing wave technique by Findlay et al. (9) and by Pellam and Squire (10) using a pulse technique. The curve of velocity versus temperature below the lambda point is especially simply described for first sound. It is essentially flat from 0°K to approximately 1°K at 239 m/sec and then bends down continuously to 216 m/sec near the lambda point.

The close connection between first and second sound was exhibited in an experiment of Lane, Fairbank and Fairbank (11), in which second sound was converted to first sound at a liquid-vapor interface (Yale Effect). At about this same time Tisza (12) showed the close theoretical interrelationship of these phenomena by deriving wave equations for both out of a common Lagrangian. The waves were shown to be sums and differences of the divergence of the vector fields formed by the displacement of normal atoms and of ground state atoms multiplied by appropriate densities. Using the equations of Tisza to explain the Yale Effect, Pellam (13) thoroughly analyzed the conversion of second sound to first sound and noticed that if second sound were to impinge on a semi-impervious region, i. e., one in which there is a large viscous drag on the normal fluid only, there would arise a new kind of thermal wave. This new wave has a velocity equal to that of first sound at 0° K and to that of second sound at the lambda point. It is this wave that would

transmit some of the heat. He also showed that the rest of the heat travels through the rouge in a highly overdamped mode.

Another way of posing this problem is by a consideration of the Thermomechanical or Fountain Effect (16). A layer of rouge is packed into a tube which is immersed in helium so that the helium bath level is above the rouge but below the top of the tube. A light is then shone onto the upper rouge surface or heat is otherwise introduced to the helium above the rouge. The result is that the helium level in the tube rises. This means that in the limit of very low frequency heating, thermal energy is somehow transmitted through the rouge. We set for ourselves then the problem of examining how this energy is transported.

The experiments in this thesis have been aimed at investigating the two modes of heat transmission with special emphasis on the thermal waves. For a semi-impervious region, varying grit sizes of emery powder (silicon carbide) were used as well as jeweller's rouge packed in densities increasing up to that attainable with a machine press. This variety provided some control over the magnitude of the viscous force on the normal fluid.

To produce and detect the waves three principal methods were employed. We used the pulse method of Pellam (7, 8), the standing wave method of Peshkov (5, 6), and finally an adaptation of the standing wave method. The importance of the search for these thermal waves arises from the consideration that the only other heat waves known are those of infrared radiation and of second sound.

I. Experimental Part

I.1 The Pulse Method

On account of its directness and ease of interpretation, it was decided to make the first attempt at observing these new thermal waves with the pulse method (8).

The electronic system for effecting the measurements is presented in Figure 11. The oscilloscope (Du Mont Radar Scope type 256-F) is set to trigger its horizontal sweep just as a trigger is sent out from it to excite a mono-stable multivibrator. This multivibrator is provided with controls to enable adjustment of both the height and length of the emergent pulse. The pulse is led into the transmitter, which is essentially a resistor, r_1 . The heat pulse, after a suitable time interval, impinges on the receiver, which is also a resistor, r_2 , through which runs a constant current I . The constancy of I is assured by connecting another resistor, R , much greater than r_2 , in series with it and some dry cells. When the heat pulse arrives at r_2 , it changes the resistance by some amount Δr_2 , which is proportional to the temperature difference between the heat pulse and the surrounding helium. The pulsed voltage, $I\Delta r_2$, is amplified by the A.C. amplifier (General Radio type 1231-B) and led into the vertical amplifier stage of the oscilloscope.

The trace on the oscilloscope consists then of one large initial pulse which is received by the receiver from the transmitter at the speed of electromagnetic waves (pickup) plus a smaller pulse received by the above described slower route through the helium. Actually, when the attenuation of the heat pulses is sufficiently low, the pulses reflect back and forth up to seven times, and this longer time interval allows correspondingly less error in the velocity computation. The horizontal sweep circuit of the radar oscilloscope is especially provided with a crystal marker generator which generates a sweep consisting of marker dots each 50 microseconds apart. When properly calibrated, this allowed measurements of pure second sound velocity to be made that were in error by only 1.5%.

The transmitter was simply a circular piece of bakelite coated with a thin carbon film of resistance 800 ohms per square. Around the periphery was painted a circle of silver paint which was grounded by means of a small screw through half of a coaxial cable, and the other half of the coaxial line fed in the pulses through a silvered terminal at the center of the disc. The receiver was identically designed and the receiver and transmitter were kept apart by an annulus of either lucite or brass, to which they were attached by small screws. The resistances of the receiver and transmitter at the temperatures of the experiment ranged approximately from 300 ohms to 500 ohms, depending on the

radius of the inner electrode and the radius of the grounded circle of silver paint. A typical element is diagrammed on Figure 13A.

Upon occasion, when the radar scope was not available, a modified circuit was used. The alternate oscilloscope (Hewlett-Packard type 130A) was triggered by a blocking oscillator which simultaneously triggered the multivibrator. This is a straightforward replacement of the internal trigger of the radar scope. The sweep scale on this alternate oscilloscope was not as constant as on the radar scope, and these measurements were consequently less reliable.

The distance of the receiver from the transmitter was varied but since, throughout the latter parts of the experiment, attenuation was a problem, it was generally fixed at 0.374 cm. The currents used in the receiver were approximately 3 milliamperes, and this made the power output at the receiver from 2 to 5 milliwatts per square centimeter. The pulse length used in the transmitter was generally 350 microseconds, and this was fed in at a repetition rate of 80 per second.

The received signals were as small as 0.15 millivolts, and the amplifier provided a gain of 15,000. This corresponds to a height of heat pulse of 0.3 millidegrees above the surrounding helium. The signal to noise for these voltages was about 2, and no signals smaller could be reliably detected.

In order to insure that the liquid helium had free access to the interior of the spacer and hence to the interstices of the rouge and

emery, a number of techniques were used. We put holes in the receiver and transmitter and placed a thin layer of glass wool to reserve a space between the heater and the rouge on both the receiver and transmitter side. All methods were equally effective and, indeed, we mostly gave the helium access through the loosely fitting receiver and transmitter periphery.

The experiments themselves are, as mentioned, straightforward, and offer no unusual difficulties. A little practice with a Polaroid camera attached to the oscilloscope made it possible to take photographic data which was analyzed after the run was over. Each of the points on Figures 1 through 10 represents a composite of four photographs of the same measurement. In all, approximately 1500 photographs were analyzed for these measurements.

To test the reliability of the apparatus and to test the meaningfulness of occasional non-passage of pulses through dense rouge, we measured the velocity of second sound through helium itself many times. Figure 1 shows these measurements.

The space between the receiver and transmitter was then filled in order with grit #46 emery powder and the velocity of heat pulses measured. This grit of powder is silicon carbide granules which pass through a sieve opening of 0.35 mm. The results are presented on Figure 2.

Figure 3 shows the same measurements carried through for grit #100 emery powder, sieve size 0.15 mm. It will be noticed that the measurements here break off at a higher temperature on the low temperature end than in the two earlier graphs. This is because the attenuation at this grit size was large enough to blot out any pulses below this.

Figures 4, 5, 6 and 7 are respectively the same curves for grit #150 (approximately 0.1 mm sieve size), grit #200, (0.075 mm sieve size), grit #320 (approximately 0.044 mm sieve size), and grit #400 (approximately 0.037 mm sieve size). The particle size of grit #600 emery powder was estimated under the microscope as 0.02 mm and Figure 8 is the result of filling the spaces with this.

Figure 9 represents the results of several runs using rouge powder of different packing density as indicated. The size of the rouge particles is not well known but has been measured under the microscope as approximately 10^{-3} mm. It will be noticed from this graph that the apparent velocity of heat pulses drops as the rouge density is increased. It was impossible to use less rouge density than the lower limit of 0.90 grams per cubic centimeter, since it would fall out of the container. At densities of 1.13 grams per cubic centimeter and larger, i. e., only 10% larger than the results indicated by the square markers, the attenuation was so large that no pulses were seen.

In an attempt to get an even finer material we packed together zeolite (Linde type 5A) crystallites (14). Although the crystal structure contains very small channels of 10 Å diameter, the crystallites themselves are 0.001 mm in diameter. Figure 10 is a plot of the apparent velocity of heat waves through helium trapped among zeolite crystallites.

I.2 Results of the Pulse Method

Let us consider what results we would expect for the velocity of heat waves if we assume the emery powder granules to be spherical and that no other physical principle is operative except that the sound goes around the spheres. Under these conditions, in order to traverse one diameter, the heat pulse must go around the half circumference of the corresponding circle instead of directly along a diameter as it would if there was no obstacle in its path. The deviated path is $\pi/2$ longer than the direct one, and the apparent velocity is $2/\pi$ times the second sound velocity. On Figures 2-8 the dotted line represents this curve.

Near the lambda point the above mechanism is adequate to describe what is happening since the measured points are rather close to the ideal curve. It is seen that as the temperature gets lower, or the grain size smaller, the experimental points diverge more and more from this dotted curve. The large errors indicated with the experimental points represent the difficulties engendered by much attenuation at these

higher grit numbers and lower temperatures.

We tentatively suggest, then, that for relatively large particles such as these, second sound degenerates to a highly attenuated wave whose velocity decreases as the particle size decreases. The attenuation of these degenerated waves increases with decreasing temperature in the range investigated and also with decreasing particle size.

There are two possible explanations for these phenomena: frictional dissipation of energy due to slippage of the normal fluid and thermal relaxation involving heat exchange with the rouge particles. It was thought to distinguish between the two by using still tighter packings of still smaller particles. On the hopeful assumption that slippage was the cause of the attenuation, we would be decreasing the slippage and would more easily be able to see the transmitted heat. As will be shown, the attenuation was determined to be the result of thermal absorption.

Figure 9 shows a continuation of this attenuation. Notice that even with fixed particle size, the velocity of the thermal pulses goes down with increased density of packing, since this decreases the channel diameters as effectively as using smaller granules would. At sufficiently large rouge densities the received signals are no longer distinguishable from the background.

The proper theory (13) of waves in helium trapped in interstices through which the normal fluid cannot move predicts in the limit of totally trapped normal fluid and no heat absorption non-attenuated waves

with a velocity independent of the flow resistance. What we have so far observed is thought to be either the result of insufficient flow resistance, i. e., the normal fluid is still free to flow and we have not yet sufficiently clamped it to prevent zero momentum flow with the wave, or the result of heat absorption. This point is discussed in detail later.

The inherent difficulty of the pulse method is that a wide-band amplifier must be used to receive the pulses. Since the minimal noise is proportional to the band width in any amplifier, it was decided to pursue the waves down to greater rouge densities and smaller channel sizes by a more sensitive means - the standing wave method.

I.3 The Standing Wave Method

In principle, the apparatus for this approach is not much different from the pulse method. The triggered multivibrator is replaced by a signal generator (Hewlett-Packard type 200CD), which has a variable output capable of providing from 0.20 volts to 25.0 volts across a 400 ohm transmitter-resistor. The receiver and transmitter system was initially the same as in the pulse method (see Fig. 13A for a typical element), but now the received signal is a heat wave. This is amplified by the same procedure as earlier and then led into a wave analyzer (General Radio type 736-A). The system was carefully grounded. Figure 12 shows a schematic diagram of the electronics.

The spacer between the receiver and transmitter now provides a resonant chamber for second sound waves, and if the transmitter is sending one of the resonant frequencies, the chamber serves effectively as a very highly selective amplifier. If the signal generator is set to send out waves of frequency ω , then the transmitter converts this to a heat signal at frequency 2ω , since the heating effect of a current is proportional to its square. It is this wave which gets sent into the cavity and for whose reception the wave analyzer is tuned at 2ω .

The measurements are then made in the following way. Initially, the signal generator is set at some very low frequency and the signal received on the wave analyzer at twice that frequency is noted. The signal generator frequency is then gradually increased while the wave analyzer is retuned each time to twice the emitted frequency. At this point the electromagnetic pickup is an aid because it enables us to tune exactly to twice the emitted frequency, since the pickup spectrum has a maximum there. We continue this tuning and retuning until we get to a resonance, at which frequency careful and accurate and reproducible measurements of the height of the received signal and of the resonant frequency itself can be made. The tuning is then continued further so as to ensure that the resonances do indeed occur at integral multiples of the first resonance, as they should.

A word about the pickup is in order. Its source is in the signal generator, and it became more of an annoyance as we put the receiver

and transmitter in more intimate proximity. For the present we were able to control it with little special effort.

Our initial attempts were to carefully standardize the technique and apparatus by measuring the velocity of pure second sound and then to fill the chamber with tightly packed rouge and repeat the same procedure. We hoped to observe new resonances at frequencies appropriate to the new thermal waves through rouge. The first part of this was very successful as Figure 14 shows. The errors associated with each of these measurements are about 1.5%, and each point is a composite of up to five resonances.

We again were careful to allow free access of helium to the rouge when we filled the container by putting a layer of glass wool between the rouge surfaces and both the receiver and transmitter, and by putting holes in the receiver and transmitter. Also, to further clamp the normal fluid, we packed the rouge with a pile driver-anvil technique in miniature so the rouge density was 2.3 gm/cm^3 . Nevertheless, when we repeated our scannings, this time with rouge, and at several temperatures below the lambda point, the resonances disappeared.

Our next attempt was with a small modification of this standing wave method. So far, we have been thwarted by our inability to get signals through the rouge. It was thought that much more fruitful results would come out of an experiment in which we had a "handle," i. e., some positive signals that could search out the rouge and come back to our

sensing elements. For this end it was decided to attempt measurements with a closed container with the receiver and transmitter at the same end. The waves would then reflect off the lucite bottom of the chamber and at resonance they would be amplified just as before in the chamber, and then picked up by a receiver concentric with the transmitter. After this method had been well understood, the rouge would be pressed in place at the bottom of the chamber, and we would look for new resonances. The design of the combined receiver-transmitter element is shown in Figure 13B.

At this stage the pickup became a really severe problem, since the receiver and transmitter were so close together. After much trial it was discovered that pickup could be reduced to reasonable proportions if sufficient care was taken to provide a low resistance path to ground for both receiver and transmitter signals. To this purpose the grounded silver paint circle was provided with other terminals. The result was that we enjoyed a signal to pickup as favorable as 8 to 1 for the remainder of this experiment.

It was, of course, necessary with this apparatus, too, to make many measurements without rouge. The results of these measurements appear on Figure 15, and their errors also are approximately 1.5%.

With this assurance that we understood our apparatus, we were finally ready for some penetrating measurements on the helium trapped

in rouge. Our plan was to fill the container with rouge to varying depths and for each case to scan over all frequencies of interest and plot up the signal received as a function of second sound frequency. During this we were especially cautious in measuring both the height and frequency of all resonances and anti-resonances. This enabled us to compare the accuracy with which the resonances occurred at integral multiples of the primary resonance. We were also eager to see how many resonances could be observed for fixed container dimensions and fixed rouge thickness, and whether the resonant frequency corresponded to a chamber depth equal to the depth before rouge was added, or to the depth after rouge was added, or to some intermediate value. In other words, does a depth of rouge d shorten the chamber length by d , by something smaller than d , or does it lengthen the chamber?

The resistance of the transmitter, for which we used the inner circle, was typically 400 ohms and the resistance of the receiver, the outer annulus, was typically 120 ohms. The receiver current was increased to 7.5 milliamps, making a power output of about 7 milliwatts per square centimeter, and approximately 14 alternating current volts were applied at the transmitter for about 80 milliwatts per square centimeter power output there.

A few runs showed that the signals came through clearest at lowest temperatures when there was no rouge in the container, so it was decided to restrict the scanning, temporarily at least, to the lowest

temperatures we could reach. This is expected to be the most interesting region anyway for our purposes, since then the helium is almost totally superfluid and only this component is likely to bring out information from the interstices of the rouge.

Figure 16 shows a typical scan taken as described above with a container 2.69 centimeters deep filled 16.0% with rouge at 1.29°K. Figure 17 shows the control scan taken with the same container but filled 16.4% with lucite at 1.328°K. A comparison of these will be made in the next section.

The flexibility of the standing wave method was extended by providing for a variable height to the chamber. This would enable sharper tuning, since we could now tune to a resonance in height as well as frequency. The essentials of the apparatus constructed for this approach are shown in Figure 18.

The rouge (R) is packed into a single block of lucite machined to the shape of the container (B). This block is attached to a supporting stand (S) provided with leveling screws (A), and the whole is suspended by thin-walled stainless steel tubes, which serve as stems extending down from the Dewar cap to which they are soldered. The receiver and transmitter element (RT) is of the type shown in Figure 13B, and it is backed up by a lucite wafer (L) for mechanical support. The electrical contacts are provided for by 0-80 flat-headed screws, which are countersunk into the face of the receiver so they do not protrude significantly. This enables

us to lower the receiver-transmitter arbitrarily close to the rouge without damaging the rouge surface. The electrical contact is made at the back of the lucite plug to coaxial cables which run up through a stainless steel tube (T). At its upper end the tube is sealed and provided with coaxial connectors to which the rest of the electronic gear is attached. The tube is carefully centered by a lucite spacer which is attached to it and which provides tracks for the supporting stems. The Dewar cap was fitted with an O-ring seal so as to permit the receiver and transmitter to be moved up and down while the helium was being pumped on and without breaking the seal. In order to measure the height of the receiver-transmitter from the rouge, a vernier scale was firmly attached to the central tube outside the Dewar, and the top of the Dewar was provided with a scale. This enabled us to measure distances to within 0.001".

It is worth noting that meaningful measurements can only be made when the helium level in the Dewar is above the uppermost edge of the block (B). When the general level falls below this, the temperature of the trapped helium rises due to the heating at the receiver-transmitter element. This decreased surface of the trapped helium prevents the pump from keeping it as cold as the helium bath and the result is, whereas the apparent level of helium in the Dewar may be well above the receiver-transmitter, there may actually be no liquid helium anywhere in the resonant chamber.

Care must be taken that the receiver-transmitter is well centered in the lucite block and also loosely fitting, since if it rubs the sides of the chamber, the silver paint loosens from the contact screws. This makes the receiver circuit exceptionally noisy, since the receiver current crossing a variable contact resistance at the terminals sends out signals.

Here, again, there was much pickup. This time we found that it could be made smallest if we grounded directly from the terminals to the steel tube, T, and if we were very careful to keep the receiver-transmitter firmly attached to the lucite wafer. The most effective means of decreasing the pickup was to let it partially cancel itself out by compensation from a dummy circuit to the receiver circuit. To do this, on the back of the receiver-transmitter are painted again the two circles which form the receiver part of the element, i. e., the two outer circles. This pair of circles differs from the true receiver very little in position (since the card is thin) and configuration (since the shapes are faithfully followed), but the resistance between them is infinite, since the back of the card is non-conducting bakelite. This means that whereas the electromagnetic pickup across these two circles is the same as on the true receiver, no second sound is picked up by them. The cancelling out is effected by connecting the circuit on the back anti-parallel to the one on the front. This reduced the low temperature pickup by a factor of almost one-half.

The first use to which this apparatus was put was to observe the lowest resonant frequency at each of several chamber heights. Since the reciprocal of the resonant frequency is directly proportional to the length of the chamber at fixed temperatures, a plot of these two should give a straight line if the container bottom is impermeable to our waves. If, however, the waves are penetrating the rouge, then the curve will not be a straight line but will turn away before it intercepts the axis. Since we already know from our earlier scans (Figs. 16 and 17) that some of the second sound is reflected back, what we would expect is both a straight line and then another curve which departs from it as the receiver-transmitter gets close to the rouge. Unfortunately, this method was complicated by the presence of much fine structure in the spectrum. The only way to detect the first maximum unequivocally is to scan with the wave analyzer and signal generator over a large frequency range and to record the signal received frequently. This was done at each of several distances and the results are plotted on Figure 19. On this figure, each of the scans is to be associated with the receiver-transmitter distance indicated by the dark line directly next to it. The distance itself may be read off from the abscissa scale. The spectra are all plotted on an arbitrary but consistent scale, and the straight line corresponding to pure second sound, reflected right off the rouge surface as if it were impermeable, radiates out from the origin and is labelled in the right hand corner. The spectra were taken at an average temperature of

1.296° K. Near this temperature the second sound velocity changes very slowly with temperature. The line beginning at 8.5 on the ordinate scale, and radiating upward, corresponds to the signals that would be received from the bottom of the container 5.16 centimeters below the surface of the rouge by the thermal waves. It will be seen that much fine structure is associated with these spectra and, in order to determine what part of the fine structure is due to information coming to us from below the rouge surface, we repeated these scans, replacing the rouge surface by a wafer of lucite. The results of these runs may be seen on Figure 20. The scale of the spectra here is the same as on Figure 19.

In order to be able to examine the region where the new thermal waves were expected without the obscuring effects of the fine structure, we decided to remove this. After some investigation, it was understood that most of the peaks and troughs, except for the pure second sound peaks, are due to excitation of cross-modes in the resonant chamber. We attempted the elimination of these by constructing an annulus of lucite which was placed exactly in the center of the rouge surface, so that when the receiver-transmitter was pushed down as far as it would go onto the ring, the receiver and transmitter would be totally insulated from each other except for communication through the rouge. The absence of the fine structure of troughs and peaks in these scans would at once prove that those in Figures 19 and 20 are due to cross-modes and

also remove these cross-modes. This new configuration also shows unequivocally any signals that come through the rouge. The spacer was 0.482 cm high and the rouge 5.06 cm deep.

Figures 21, 22, and 23 show the results of these scans at one rouge thickness and at three temperatures. Other temperatures were tried as well as another rouge thickness, but the results were the same. It will be noticed that the second sound signal that is received is very much weakened and only comes through at all because of a small off-centeredness of the receiver-transmitter. All of these curves were extended far to the right without observing any other peaks.

I.4 Results of the Standing Wave Method

Our inability to see wave resonances in the chamber formed between the receiver and transmitter and packed with rouge was indication that the wave was being degraded in some way in the rouge so as to destroy it. This was not too surprising, since separation of the receiver and transmitter means that the wave has to get entirely through the packed rouge before it will be detected. This difficulty is avoided by using the surface of the rouge as a reflector for second sound.

Now we have a two-pronged approach. Any wave that gets through the rouge will be reflected from the lucite bottom, and from thence to our receiver by the same route along which it came, and any wave that

cannot get through and "turns back" will also get back to the receiver. Also, by comparing the results of reflection from a rouge surface and from a lucite surface, we can get a measure of just how much energy is lost in the rouge and perhaps get a hint as to what happens to it. The Figures 16 and 17, which show the results of this experiment, will now bear some examining. The most striking thing a comparison of these two spectra indicates is that they are qualitatively extremely similar. Indeed, there is barely a feature on one curve's profile that is not repeated on the other. This means that all of the fine structure is due to things like coupling in cross-modes of various orders and phase sensitive interference between the background pickup and the second sound resonances. There is one quantitative difference that bears note, however. The resonances from the lucite bottom are significantly more slowly damped than are the resonances from the container with a rouge bottom. We notice, in fact, that even though the initial resonance from the lucite (150 microvolts) is smaller than the initial resonance from the rouge (180 microvolts), the former spectrum clearly exhibits at least 7 overtones, whereas the latter exhibits only 6. This means that the rouge is not quite a hard surface to second sound waves. Some of the heat energy in the second sound is entering the rouge but not coming back as waves. Once again we see that too much of the heat is being degraded to get back to our receiver. We also notice that the waves which do get reflected

back from the rouge surface show exactly the resonance frequencies which are expected from a rigid bottom. The answer, then, to the question posed regarding this problem in the last section is that for part of the second sound energy the rouge does shorten the chamber by the height d of the rouge column, but for the rest of the second sound energy, the effect of the rouge is to absorb it, i. e., to infinitely lengthen the chamber.

The measurements with the apparatus of Figure 18 provided the most penetrating results we were able to achieve. The movable tube enabled us to tune more sharply to the resonances than was possible with only tuning in frequency as before. This in turn made it possible for us now to discern more clearly the position of the maximum responses and hence the velocity of second sound could be more reliably determined. We now also perceive that there is more fine structure on the spectra (Fig. 19) than before. In order to separate out the fine structure that is due to the rouge from that due to spurious causes, we examine Figure 20. Notice that all of the features of the spectra are faithfully repeated; indeed, the same peaks and valleys appear on Figure 20 even more pronounced than with a rouge base. There is, however, a significant difference between the sets of spectra quantitatively, just as earlier. The reflections from the lucite surface are much stronger than from the rouge. Consider the scans at the 0.124" high chamber. The lucite bottom gives a peak second sound resonance of 90 microvolts, while

from the rouge only 50 microvolts return to the receiver. The background noise level was 0.5 microvolts throughout. This means that even if our new thermal waves were to account for a temperature difference in the chamber of 2 microdegrees, they would be visible on our scans of Figures 19 and 21, 22, and 23.

We notice that our comparison of Figures 19 and 20 gives the same results as of Figures 16 and 17. In both pairs of cases, although there is ample evidence that the heat is entering the trapped helium, there is no evidence of its conversion to the waves we expect from theory. The waves, then, do not appear because the heat propagation is being absorbed before any resonance is built up.

In order to test our understanding of the spurious troughs and peaks as being due to a mixture of phase interference between the pickup and resonance and excited cross-modes, we notice that on the Figures 21, 22, and 23 this fine structure disappears. The only difference in measuring techniques is to destroy the cross-mode resonances with the annulus. On these latter three figures we have drawn the frequency at which we would expect resonance to occur according to theory. The absence of the fine structure shows us unequivocally that the waves do not show up to within our sensitivity. All of these scans were extended far to the right so that we might see waves twice as slow.

It is instructive to note that all of the second sound resonances are preceded by a deep trough, sometimes two. This is especially

clearly seen in Figure 21 and in those scans on Figure 19 which correspond to short chamber lengths. Indeed, in these last the resonance is so much obscured by the dips that the main feature of the resonance is a decrease rather than an increase in signal received. The decrease is only an apparent one and is due to the electronic pickup and resonant frequency interfering with each other. It does not cut down our sensitivity unless the resonances of the new waves are in a particularly unpropitious phase relation to the pickup. We have eliminated this difficulty by trying more than one rouge thickness and by looking for the new waves at several different temperatures, so that the expected resonant frequencies cover many regions.

II. Theoretical Part

Our task here is to rigorously examine the consequences of damping the normal fluid of the liquid helium while leaving the superfluid free. This corresponds to the experimental cases we have examined wherein the damping is provided by the rouge particles. The relations we derive here were first derived by Pellam (13) in 1948. We offer a somewhat simpler method.

We start with the equations of first and second sound as derived by Tisza (12):

$$\frac{\partial^2}{\partial t^2} (\nabla \cdot \xi_1) = c_1^2 \nabla^2 (\nabla \cdot \xi_1) \quad (1)$$

$$\frac{\partial^2}{\partial t^2} (\nabla \cdot \xi_2) = c_2^2 \nabla^2 (\nabla \cdot \xi_2) \quad (2)$$

where c_1 and c_2 are the velocities of first and second sound. They are functions of temperature alone. If we let ρ_n , ρ_s and ρ stand for the normal fluid density, the superfluid density, and the total density, respectively, and if we let ξ_n and ξ_s represent vector fields, the components of which represent the displacement of the normal fluid and superfluid, respectively, in the component direction, from their equilibrium positions, we have as definitions for ξ_1 and ξ_2 :

$$\xi_1 = (\rho_n \xi_n + \rho_s \xi_s) / \rho \quad (3)$$

$$\xi_2 = (\xi_n - \xi_s) \rho_s / \rho \quad (4)$$

Since in our experiments the only heat flow is in the z-direction of cylindrical coordinates, the only non-zero components of ξ_1 and ξ_2 are those in this direction. If we then perform a partial integration on z and call the z-components by the scalar notations ξ_1 and ξ_2 , we have the new simpler equations:

$$\ddot{\xi}_1 = c_1^2 \nabla^2 \xi_1 \quad \text{First sound} \quad (5)$$

$$\ddot{\xi}_2 = c_2^2 \nabla^2 \xi_2 \quad \text{Second sound} \quad (6)$$

Tisza has pointed out that the first of these relations has the physical meaning of a net flow of matter at constant entropy, while the second corresponds to a flow of entropy at constant density. In order for us to put a damping force on the normal fluid, we must re-express these equations in terms of ξ_n and ξ_s where these scalar variables are the z-components of their respective vectors.

Substituting then into equations 5 and 6, we have the new equations:

$$\frac{\rho_n}{\rho} \ddot{\xi}_n + \frac{\rho_s}{\rho} \ddot{\xi}_s = c_1^2 \frac{\rho_n}{\rho} \nabla^2 \xi_n + c_1^2 \frac{\rho_s}{\rho} \nabla^2 \xi_s \quad (7)$$

$$\frac{\rho_s}{\rho} \ddot{\xi}_n - \frac{\rho_s}{\rho} \ddot{\xi}_s = c_2^2 \frac{\rho_s}{\rho} \nabla^2 \xi_n - c_2^2 \frac{\rho_s}{\rho} \nabla^2 \xi_s \quad (8)$$

If we now first simply add these equations and then multiply equation 7 by ρ_s and equation 8 by ρ_n and subtract, we get the two wave-like equations in ξ_n and ξ_s that we sought:

$$\ddot{\xi}_n = \left(\frac{\rho_n c_1^2 + \rho_s c_2^2}{\rho} \right) \nabla^2 \xi_n + \frac{\rho_s}{\rho} (c_1^2 - c_2^2) \nabla^2 \xi_s \quad (9)$$

$$\ddot{\xi}_s = \frac{\rho_n}{\rho} (c_1^2 - c_2^2) \nabla^2 \xi_n + \left(\frac{\rho_s c_1^2 + \rho_n c_2^2}{\rho} \right) \nabla^2 \xi_s \quad (10)$$

and when we put in a friction term on the normal fluid, we get:

$$\ddot{\xi}_n = \left(\frac{\rho_n c_1^2 + \rho_s c_2^2}{\rho} \right) \nabla^2 \xi_n + \frac{\rho_s}{\rho} (c_1^2 - c_2^2) \nabla^2 \xi_s - \frac{R \dot{\xi}_n}{\rho_n} \quad (9a)$$

while equation 10 stays unchanged. We have set the resistive force proportional to the velocity of the normal fluid displaced from equilibrium and have normalized so that $R \dot{\xi}_n$ is a force on the normal fluid per unit volume of normal fluid. In order to solve these equations 9a and 10 so that the results are more meaningful, we invert equations 3 and 4 and re-express 9a and 10 in the old variables. This operation gives:

$$\ddot{\xi}_1 + \frac{R}{\rho} \dot{\xi}_1 - c_1^2 \nabla^2 \xi_1 = - \frac{R \dot{\xi}_2}{\rho} \quad (11)$$

$$\ddot{\xi}_2 + \frac{\rho_s R}{\rho \rho_n} \dot{\xi}_2 - c_2^2 \nabla^2 \xi_2 = - \frac{\rho_s R}{\rho \rho_n} \dot{\xi}_1 \quad (12)$$

Now we solve these equations for waves by assuming solutions of the form:

$$\xi_1 = \xi_{10} e^{-2\pi\nu it} e^{ax} \quad (13)$$

$$\xi_2 = \xi_{20} e^{-2\pi\nu it} e^{ax} \quad (14)$$

We have here assumed that both waves have the same attenuation and frequency, as is conventional. This substitution leads to the pair of homogeneous simultaneous equations:

$$- [(2\pi\nu)^2 + 2\pi\nu iR/\rho + c_1^2 a^2] \xi_{10} - 2\pi\nu iR/\rho \xi_{20} = 0 \quad (15)$$

$$- \frac{2\pi\nu i \rho_s R}{\rho \rho_n} \xi_{10} - [(2\pi\nu)^2 + \frac{2\pi\nu i \rho_s R}{\rho \rho_n} + c_2^2 a^2] \xi_{20} = 0 \quad (16)$$

In order for there to exist a non-trivial solution for ξ_{10} and ξ_{20} , the determinant of the coefficients must vanish. This leads to the following quadratic equation in a^2 :

$$\begin{aligned}
 (a^2)^2 + [(2\pi\nu)^2 \left(\frac{1}{c_1^2} + \frac{1}{c_2^2} \right) + \frac{2\pi\nu iR}{\rho} \left(\frac{1}{c_1^2} + \frac{\rho_s}{\rho_n c_2^2} \right)] (a^2) \\
 + \frac{(2\pi\nu)^4}{c_1^2 c_2^2} + \frac{(2\pi\nu)^3 iR}{c_1^2 c_2^2 \rho_n} = 0
 \end{aligned} \tag{17}$$

If we solve this equation for (a^2) exactly, by use of the quadratic formula, we get the two solutions:

$$\left(\frac{a}{2\pi\nu} \right)^2 = - \frac{1}{2} \left(\frac{1}{c_1^2} + \frac{1}{c_2^2} \right) - \frac{iR(\rho_n c_2^2 + \rho_s c_1^2)}{2(2\pi\nu)\rho\rho_n c_1^2 c_2^2} \tag{18}$$

$$\pm \left\{ \left[\frac{1}{2} \left(\frac{1}{c_1^2} - \frac{1}{c_2^2} \right) + \frac{iR(\rho_n c_2^2 + \rho_s c_1^2)}{2(2\pi\nu)\rho\rho_n c_1^2 c_2^2} \right]^2 - \frac{Ri\rho_s \left(\frac{1}{c_1^2} - \frac{1}{c_2^2} \right)}{(2\pi\nu)\rho\rho_n c_2^2} \right\}^{\frac{1}{2}}$$

which is true for all R , large or small.

In order to better identify the modes that we will be computing, we must now notice that if $R = 0$, i. e., the helium is not trapped, then we have for the plus and minus signs the solutions:

$$\text{plus sign} \quad a^2 = - \frac{(2\pi\nu)^2}{c_2^2} \quad \text{or} \quad a = \pm i \frac{2\pi\nu}{c_2} \tag{19}$$

minus sign
$$a^2 = - \frac{(2\pi\nu)^2}{c_1^2} \quad \text{or} \quad a = \pm i \frac{2\pi\nu}{c_1} \quad (20)$$

The plus sign solution corresponds to second sound and the minus sign solution corresponds to first sound.

We rewrite equation 18 in a form suitable for binomial expansion as:

$$\left(\frac{a}{2\pi\nu}\right)^2 = -\frac{1}{2}\left(\frac{1}{c_1} + \frac{1}{c_2}\right) - \frac{iR(\rho_n c_2^2 + \rho_s c_1^2)}{2(2\pi\nu)\rho\rho_n c_1^2 c_2^2} + \left[\frac{1}{2}\left(\frac{1}{c_1} - \frac{1}{c_2}\right) + \frac{iR(\rho_n c_2^2 + \rho_s c_1^2)}{2(2\pi\nu)\rho\rho_n c_1^2 c_2^2} \right]. \quad (21)$$

$$\left\{ 1 - \frac{Ri\rho_s \left(\frac{1}{c_1} - \frac{1}{c_2}\right)}{(2\pi\nu)\rho\rho_n c_1^2 c_2^2 \left[\frac{1}{2}\left(\frac{1}{c_1} - \frac{1}{c_2}\right) + \frac{iR(\rho_n c_2^2 + \rho_s c_1^2)}{2(2\pi\nu)\rho\rho_n c_1^2 c_2^2} \right]} \right\}^{\frac{1}{2}}$$

Now a formal expansion is carried out and we notice the unusual circumstance that our expansion is valid in the limit of both very large and very small R .

$$\left(\frac{a}{2\pi\nu}\right)^2 = -\frac{1}{2}\left(\frac{1}{c_1} + \frac{1}{c_2}\right) - \frac{iR(\rho_n c_2^2 + \rho_s c_1^2)}{2(2\pi\nu)\rho\rho_n c_1^2 c_2^2} + \left[\frac{1}{2}\left(\frac{1}{c_1} - \frac{1}{c_2}\right) + \frac{iR(\rho_n c_2^2 + \rho_s c_1^2)}{2(2\pi\nu)\rho\rho_n c_1^2 c_2^2}\right]. \quad (22)$$

$$\cdot \left\{ 1 - \frac{iR\rho_s\left(\frac{1}{c_1} - \frac{1}{c_2}\right)}{2(2\pi\nu)\rho\rho_n c_1^2 c_2^2 \left[\frac{1}{2}\left(\frac{1}{c_1} - \frac{1}{c_2}\right) + \frac{iR(\rho_n c_2^2 + \rho_s c_1^2)}{2(2\pi\nu)\rho\rho_n c_1^2 c_2^2}\right]^2} + \dots \right.$$

We are especially interested in the limit of large R , since that corresponds to tightly packed rouge.

The simplest case is for the minus sign solution, so we take it first. Collecting all terms linear in R and those not containing R , we have the two most important terms in the whole expansion:

$$\left(\frac{a}{2\pi\nu}\right)^2 = \frac{-iR(\rho_n c_2^2 + \rho_s c_1^2)}{(2\pi\nu)\rho\rho_n c_1^2 c_2^2} - \frac{(\rho_n c_2^4 + \rho_s c_1^4)}{c_1^2 c_2^2 (\rho_n c_2^2 + \rho_s c_1^2)} + \dots \quad (23)$$

This is the solution corresponding to first sound in clamped normal fluid. It represents very damped waves.

Let us now examine the case of the plus sign in equation 22 and for large R . For this case the terms linear in R cancel, and the leading term is that without R :

$$\left(\frac{a}{2\pi\nu}\right)^2 = -\frac{\rho}{\rho_n c_2^2 + \rho_s c_1^2} + i \frac{(2\pi\nu)^2 \rho_s \rho_n (c_2^2 - c_1^2)^2}{R c_2^2 \rho \left(\frac{\rho_n c_2^2 + \rho_s c_1^2}{\rho^2}\right)^2} + \dots \quad (24)$$

This means that the second sound mode becomes an undamped wave with velocity

$$\bar{v} = \left[\frac{\rho_n c_2^2 + \rho_s c_1^2}{\rho} \right]^{\frac{1}{2}} \quad (25)$$

and attenuation:

$$a = + \frac{(2\pi\nu)^2 \rho_s \rho_n (c_2^2 - c_1^2)^2}{2R \rho \bar{v}^3 c_2^2} \quad (26)$$

It is easy to see that for very large R the attenuation vanishes. Notice also that a is proportional to ν^2 and \bar{v}^{-3} just as normal attenuation. If we examine equation 9a, we can see that by very large R we mean:

$$R \gg (2\pi\nu)\rho_n \quad (27)$$

The velocity predicted by equation 25 is plotted on Figure 24. Notice that at low temperatures \bar{v} approaches the velocity of first sound, since ρ_s approaches ρ and ρ_n approaches zero, and near the lambda point \bar{v} approaches the velocity of second sound, since ρ_n approaches ρ and ρ_s disappears.

To get insight into the motion of the fluids for each of the modes computed, we merely substitute equations 13 and 14 into 11 and 12, and simplify:

$$[c_1^2(a_{10}^2 - a_{10}^2) + 2\pi\nu iR/\rho] \xi_{10} = - \frac{2\pi\nu iR}{\rho} \xi_{20} \quad (28)$$

$$[c_2^2(a_{20}^2 - a_{20}^2) + 2\pi\nu i \frac{R\rho_s}{\rho\rho_n}] \xi_{20} = - \frac{2\pi\nu i R\rho_s}{\rho\rho_n} \xi_{10} \quad (29)$$

where for convenience we have let $a_{10} = 2\pi\nu i/c_1$ and $a_{20} = 2\pi\nu i/c_2$.

In the limit R/ρ approaches infinity we have:

$$\xi_{10} = \pm \xi_{20} \text{ as the two possible modes.}$$

The first of these is a forbidden mode, since if $\xi_{10} = + \xi_{20}$, it may be shown that both must vanish identically. This is the overdamped mode that corresponds to second sound.

The second mode is a possible one. Indeed, if $\xi_{10} = -\xi_{20}$, we are led to the conclusion 25. This is the mode that represents the waves we sought. We can see this by noticing that the condition $\xi_{10} = -\xi_{20}$ implies, from equations 3 and 4, that $\xi_n = 0$, i. e., the normal fluid is clamped.

The Figures 2 through 10 show that the emery powder and rouge introduce a slowing down of the velocity of thermal waves beyond the factor of $2/\pi$ which we expect. Since the subsequent investigation of the tightly packed rouge showed no wave motion, due to heat absorption

by the rouge, we may modify our initial suspicions on this slowed-down wave velocity and attribute it to the onset of thermal absorption by the rouge rather than to insufficient viscous force on the normal fluid. The effect of a decreasing velocity of waves due to passage through an attenuative medium is well known in acoustics, but usually this effect is much less pronounced than in our case. Since in our past treatment no heat absorption has been taken into account, we here analyze the effect of the rouge as pure capacitative heat sinks. We will show that this is controlling the measurements.

If in liquid helium a temperature decrement ΔT exists, it gives rise to a heat flux \dot{H} and these are related by:

$$\dot{H} = (\rho c_v v_2') \Delta T \quad (30)$$

where ρ is the liquid density, v_2' is the velocity of thermal waves in the medium, and c_v is the specific heat of liquid helium.

The thermal impedance of the liquid may then be expressed as:

$$Z_{th} = 1/\rho v_2' c_v \quad (31)$$

In analogy with the electrical case of waves on a transmission line we define a thermal inductance L_{th} and a thermal capacitance C_{th} such that:

$$Z_{th} = \sqrt{L_{th}/C_{th}} \quad (32)$$

and

$$v_2' = 1/\sqrt{L_{th} C_{th}} \quad (33)$$

These lead us to the following equations for the thermal variables:

$$L_{th} = 1/\rho c_v v_2'^2 \quad (34)$$

$$C_{th} = \rho c_v \quad (35)$$

The physical meaning of the thermal capacitance is clear. It is the amount of heat necessary to raise unit volume of the helium by one degree. Since in our case we have rouge present besides the helium, we must add to the thermal capacity a term for it. This term will be temperature dependent and, indeed, since it is proportional to the specific heat of a solid at low temperatures, it is expected to be proportional to T^3 . We assume, then, that our new thermal capacity is of the form:

$$C_{th}' = \rho c_v + C_o \quad (36)$$

The new velocity of thermal waves is then:

$$v = \frac{1}{\sqrt{L_{th} C_{th}}} = \frac{1}{\sqrt{\frac{1}{v_2'^2} + \frac{C_o}{\rho c_v v_2'^2}}} = \frac{v_2'}{\sqrt{1 + C_o / \rho c_v}} \quad (37)$$

This may be rewritten as:

$$\left(\frac{v_2'}{v}\right)^2 = 1 + C_o / \rho c_v \quad (38)$$

At the temperatures of the experiments, ρ is effectively constant and c_v is proportional to $T^{5.5}$, so we have:

$$\left(\frac{v_2'}{v}\right)^2 = 1 + AT^{-5/2} \quad (39)$$

Since, in the absence of any thermal effects, the velocity of heat waves is still $\frac{2}{\pi}$ times the second sound velocity through pure helium, we must here understand by v_2' this reduced value of the second sound velocity.

We have plotted equation 39 in Figures 25 and 26 for a typical emery powder size and for the highest rouge density which permitted observable passage to the pulses. Since the ordinate axis is $\left(\frac{v_2'}{v}\right)^2$ and the abscissa is $T^{-5/2}$, we expect from our theory that the plotted points will lie on a straight line with slope A and ordinate intercept unity. The scatter of the points and the large associated errors make the situation far from ideal, but it will be seen that a straight line fits the data

better than any other simple curve.

Let us now solve equation 38 for v^2 . This gives

$$v^2 = \frac{v_2'^2}{1 + C_o / \rho c_v} \quad (40)$$

The effect of thermal absorption is to change the square of the thermal wave velocity by the factor $(1 + C_o / \rho c_v)^{-1}$. Let us then take as a rough approximation to the effect of heat absorption on equation 25 that the square of the second sound velocity is changed by this same factor. If we then substitute into equation 25, we get:

$$v = \left[\frac{\rho_n}{\rho} \frac{c_2^2}{1 + \frac{C_o}{\rho c_v}} + \frac{\rho_s}{\rho} c_1^2 \right]^{\frac{1}{2}} \quad (41)$$

This amounts to only unimportant changes in the expected velocity.

Our data show that the term C_o / c_v becomes important only after $\frac{\rho_n}{\rho}$ has become so small that the term $\frac{\rho_s}{\rho} c_1^2$ dominates the bracketed expression.

III. Conclusions

We have shown that the waves of Figure 24 and equation 25 are not observable under our conditions of measurement to within two orders of magnitude of the height of second-sound waves under similar conditions. The possible reasons for this unobservability are many, and we shall discuss them. The discussion naturally groups itself into two parts, limitations on the derivation and limitations on the apparatus, and they will be discussed in this order.

The most obvious apparent difficulty with the theory is that R , the viscosity coefficient, may not be large enough. Although, admittedly, not enough is known about the structure of the packed rouge and the mechanics of flow of helium in the channels to permit a responsible calculation, there is ample experimental evidence that the normal fluid is effectively clamped. The most sensitive experiment for detecting normal fluid flow through packed rouge is due to Pellam and Craig (15). In it, lift on an airfoil in a superfluid wind tunnel is sought. This tunnel was formed in the chamber between two packings of rouge and the superfluid component was made to flow by a heater. The test of lift on an airfoil is a very sensitive one for presence of viscosity and hence normal fluid flow in the chamber and the absence of lift shows that the only component of liquid helium to get through rouge is the superfluid component.

The next apparent difficulty is that the viscous force may vary some other way than linearly in the velocity of the displaced normal fluid. Judging from all the other surprising facts that have been discovered about the flow properties of liquid helium, this could conceivably be the case, although it is not likely. We believe, however, that the non-observability of the waves is due to experimental limitations.

The essence of the trouble is that temperature differences in rouge are brought to equilibrium by a diffusive equation and not by a wave equation. This means that the rouge in the bottom of the resonance chamber is constantly taking away the heat that we are putting in, and in this way destroying the resonance. From a study of the rouge density we concluded that in our last experiments the rouge accounts for half of the volume of the space wherein the new thermal waves are expected and, since the particles are small, there is ample surface for heat exchange and consequent degradation. The best way to avoid this would be to find a substance which is as suitable as rouge in all ways and also has a much lower heat conductivity at these temperatures.

Lastly, let us with hindsight examine the Fountain Effect and how it starts up. The heat signals that are transmitted through the rouge are highly dispersed by the time they get to the other end. This means that if the heat input as a function of time is a step function, for example, the flow of helium toward the heat source through the rouge

would be some highly dispersed function of time different from a step function. If, on the other hand, we could use as a semi-permeable material something that didn't absorb heat, the heat flow would be undispersed.

The exact form of the dispersion could be determined by using a very long, tightly packed rouge column and observing the fluid flow rate through the rouge that is brought forth by a fixed heat source wave form.

References

1. London, F., Phys. Rev., 54, 947-954 (1938).
2. Tisza, L., J. Phys. Radium, 1, 164-172 (1940).
3. Tisza, L., J. Phys. Radium, 1, 350-358 (1940).
4. Landau, L. D., J. Phys. U.S.S.R., 5, 71-90 (1941).
5. Peshkov, V., J. Phys. U.S.S.R., 8, 381 (1944).
6. Peshkov, V., J. Phys. U.S.S.R., 10, 389-398 (1946).
7. Pellam, J. R., Phys. Rev., 74, 841 (1948).
8. Pellam, J. R., Phys. Rev., 75, 1183-1194 (1949).
9. Findlay, J. C., Pitt, A., Grayson Smith, H., and Wilhelm, J. O., Phys. Rev., 54, 506-509 (1938).
10. Pellam, J. R., and Squire, C. F., Phys. Rev., 72, 1245-1252 (1947).
11. Lane, C., Fairbank, H. A., and Fairbank, W. M., Phys. Rev., 71, 600-605 (1947).
12. Tisza, L., Phys. Rev., 72, 838-854 (1947).
13. Pellam, J. R., Phys. Rev., 73, 608-617 (1948).
14. Broussard, L., and Shoemaker, D. P., J. Am. Chem. Soc., 82, 1041-1051 (1960).
15. Pellam, J. R., and Craig, P. P., Phys. Rev., 108, 1109-1112 (1957).
16. Allen, J. F., and Jones, H., Nature, Lond., 141, 243-244 (1938).

FIGURES

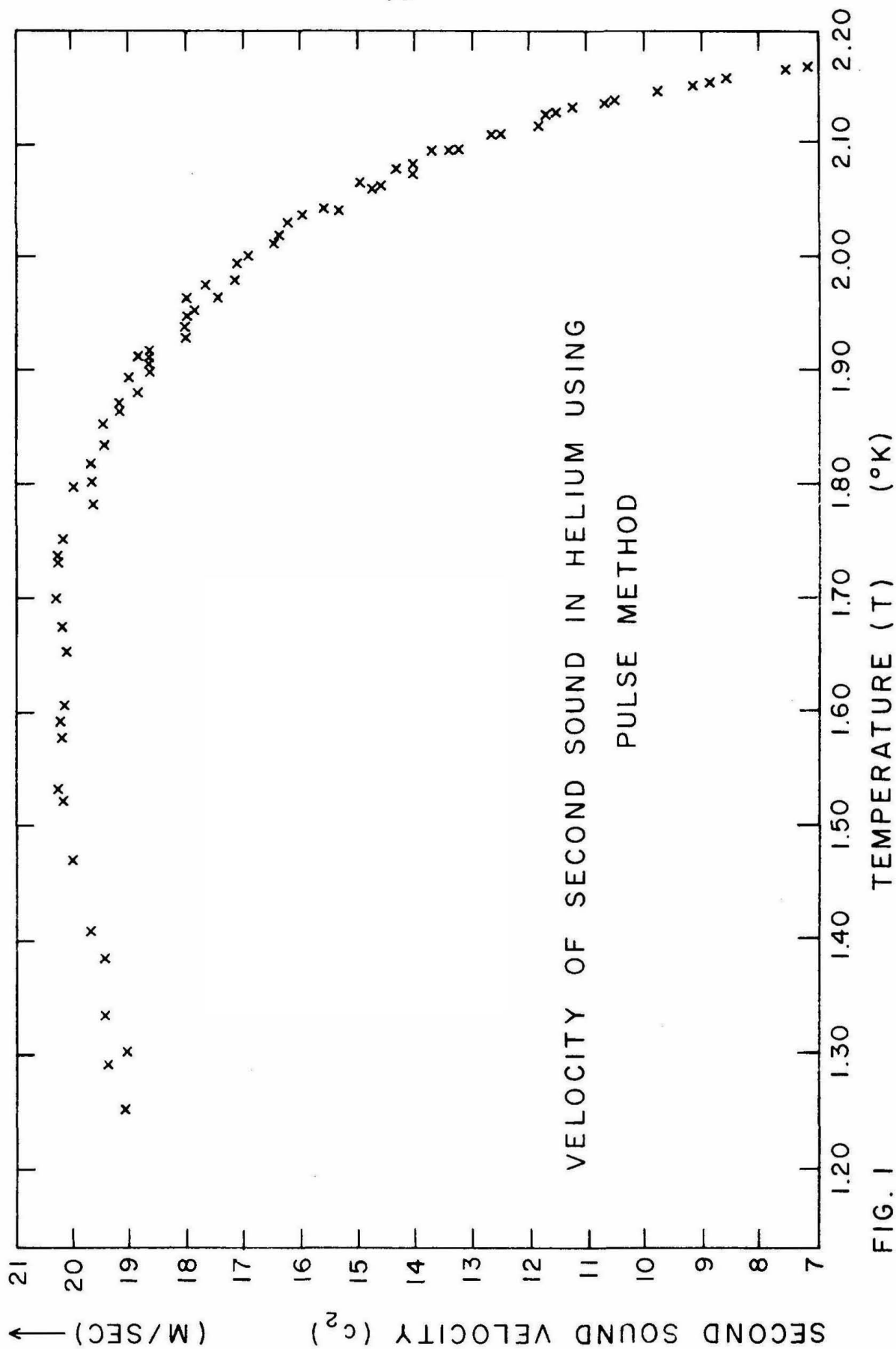


FIG. 1

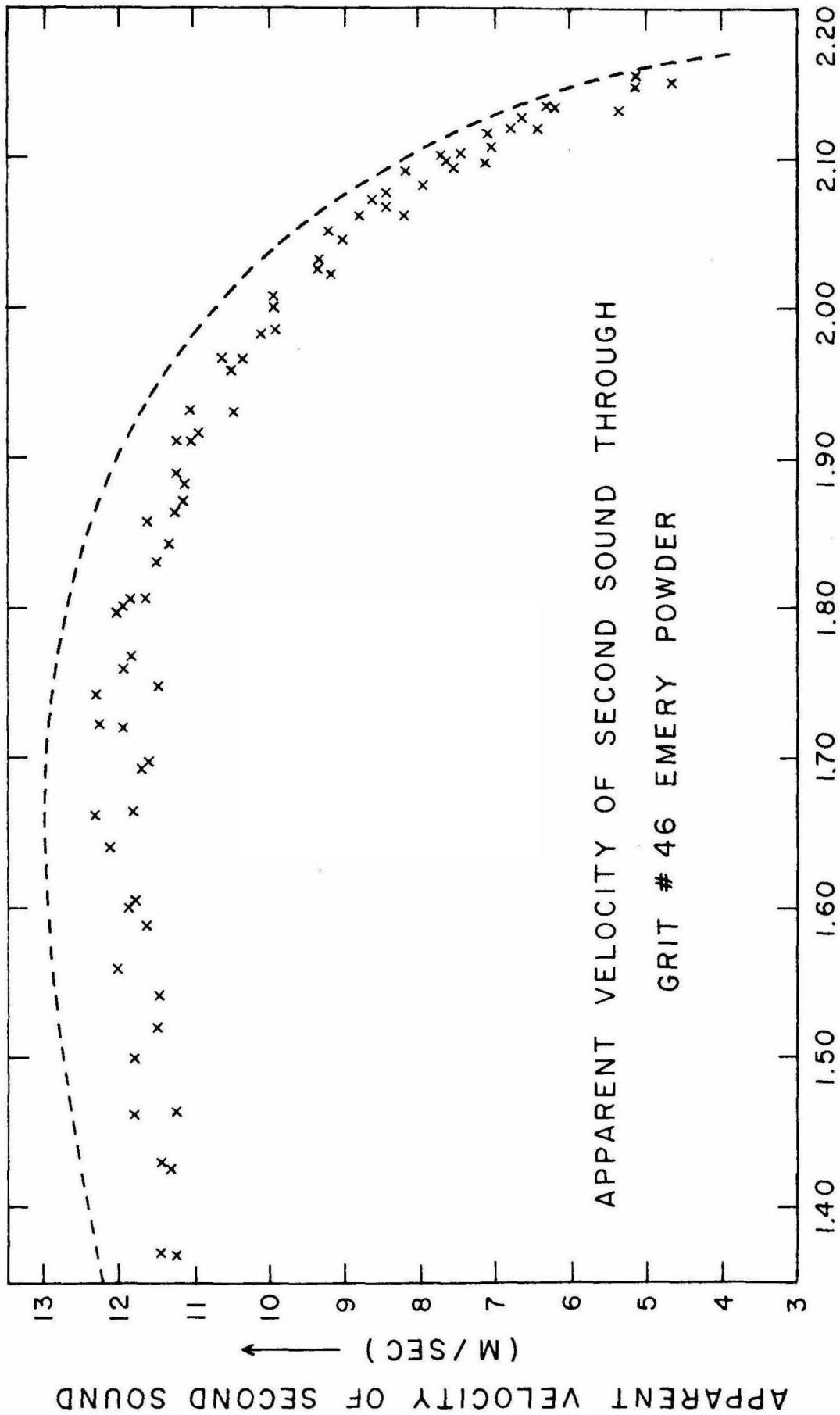


FIG. 2

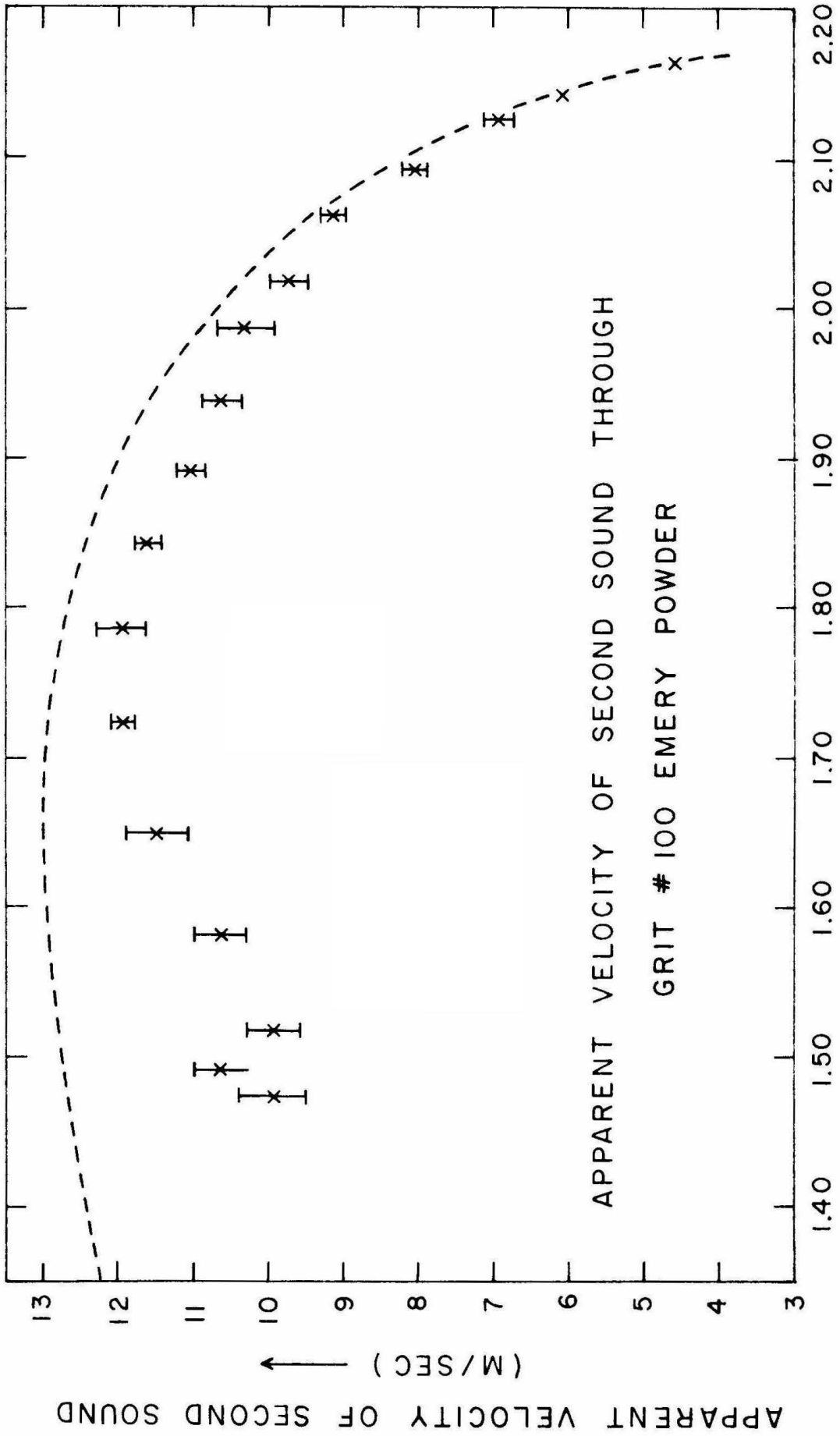


FIG. 3

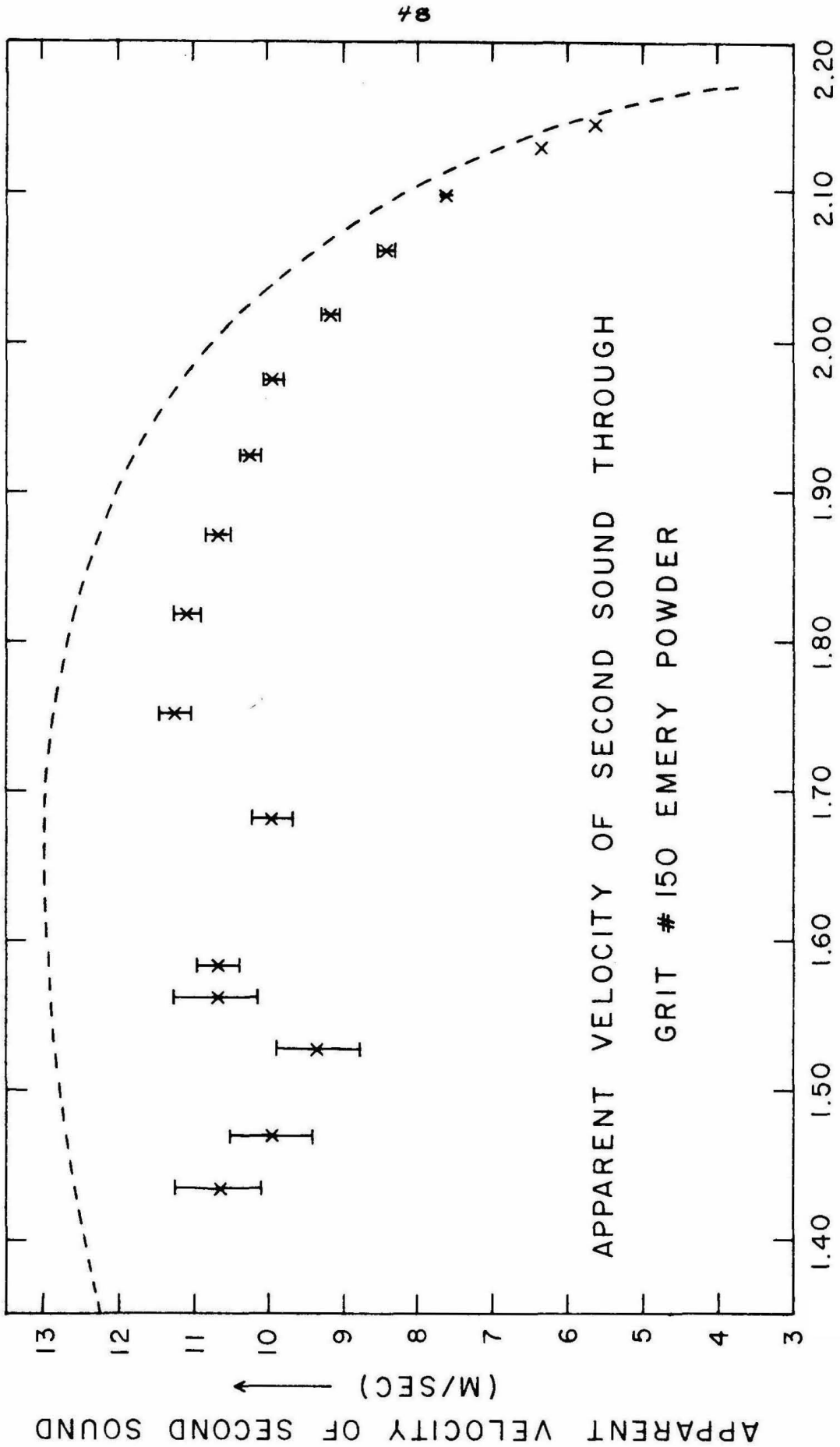


FIG. 4 TEMPERATURE (T) (°K)

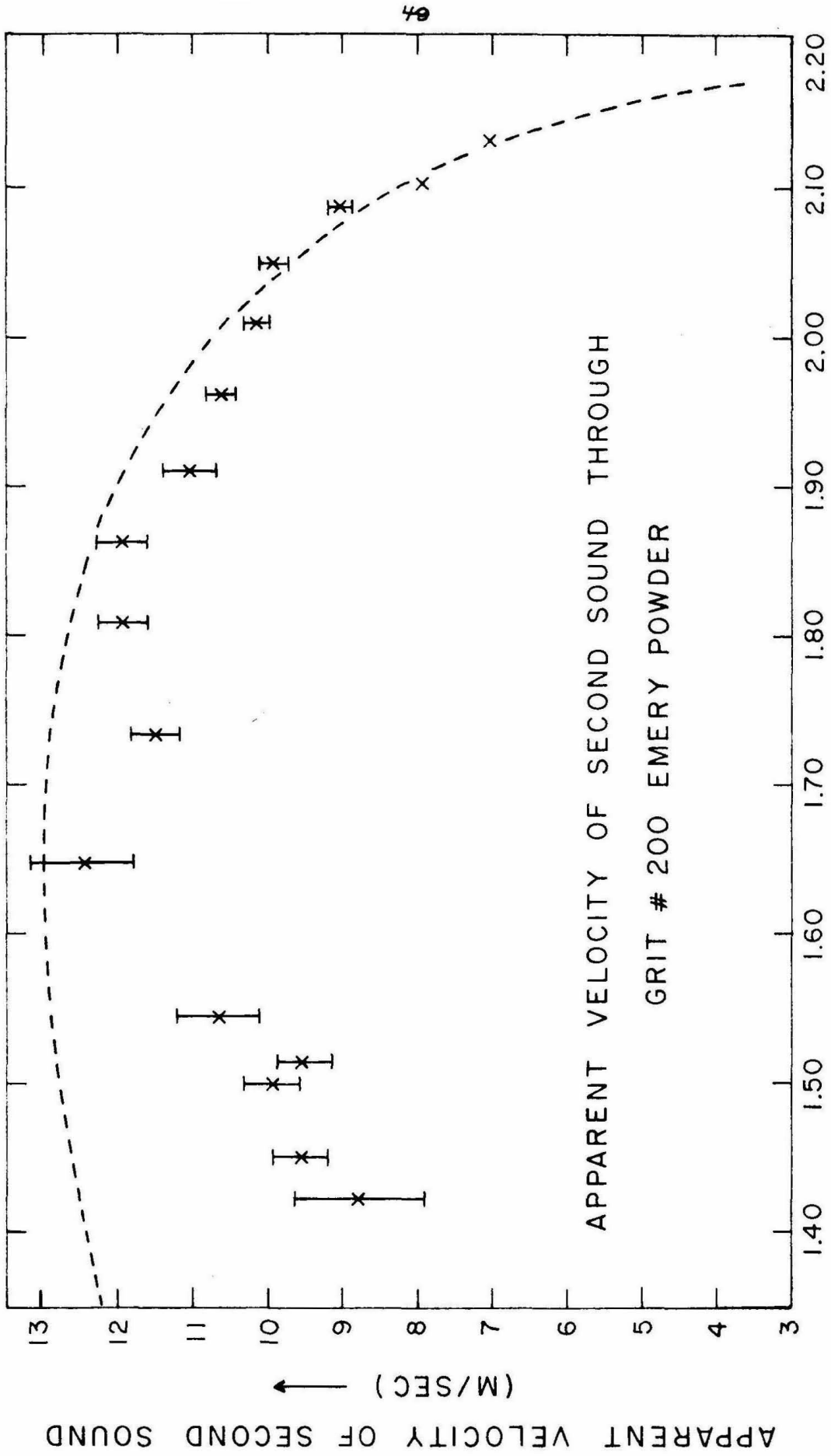


Fig. 5 TEMPERATURE (T) (°K)

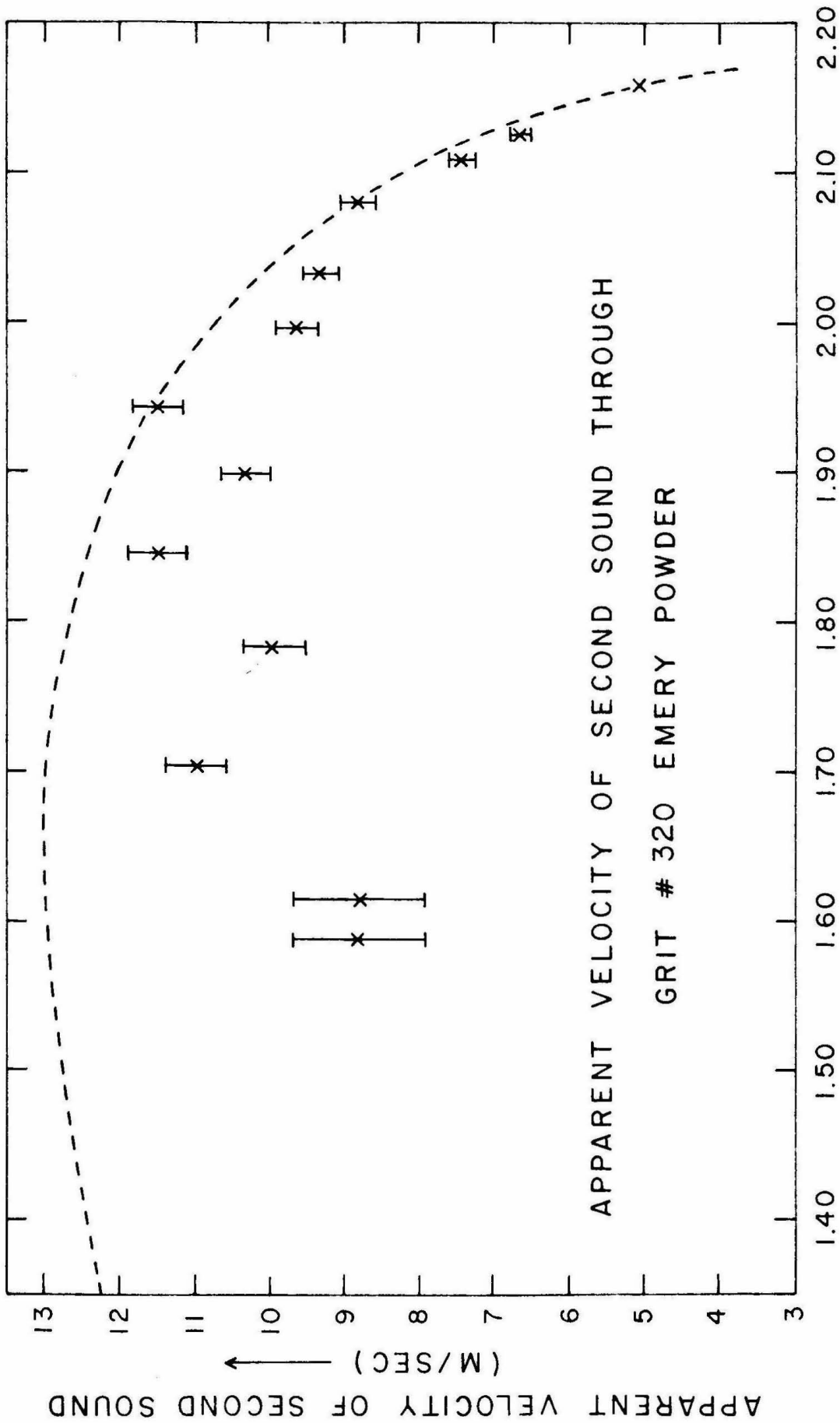


FIG. 6 TEMPERATURE (T) (°K)

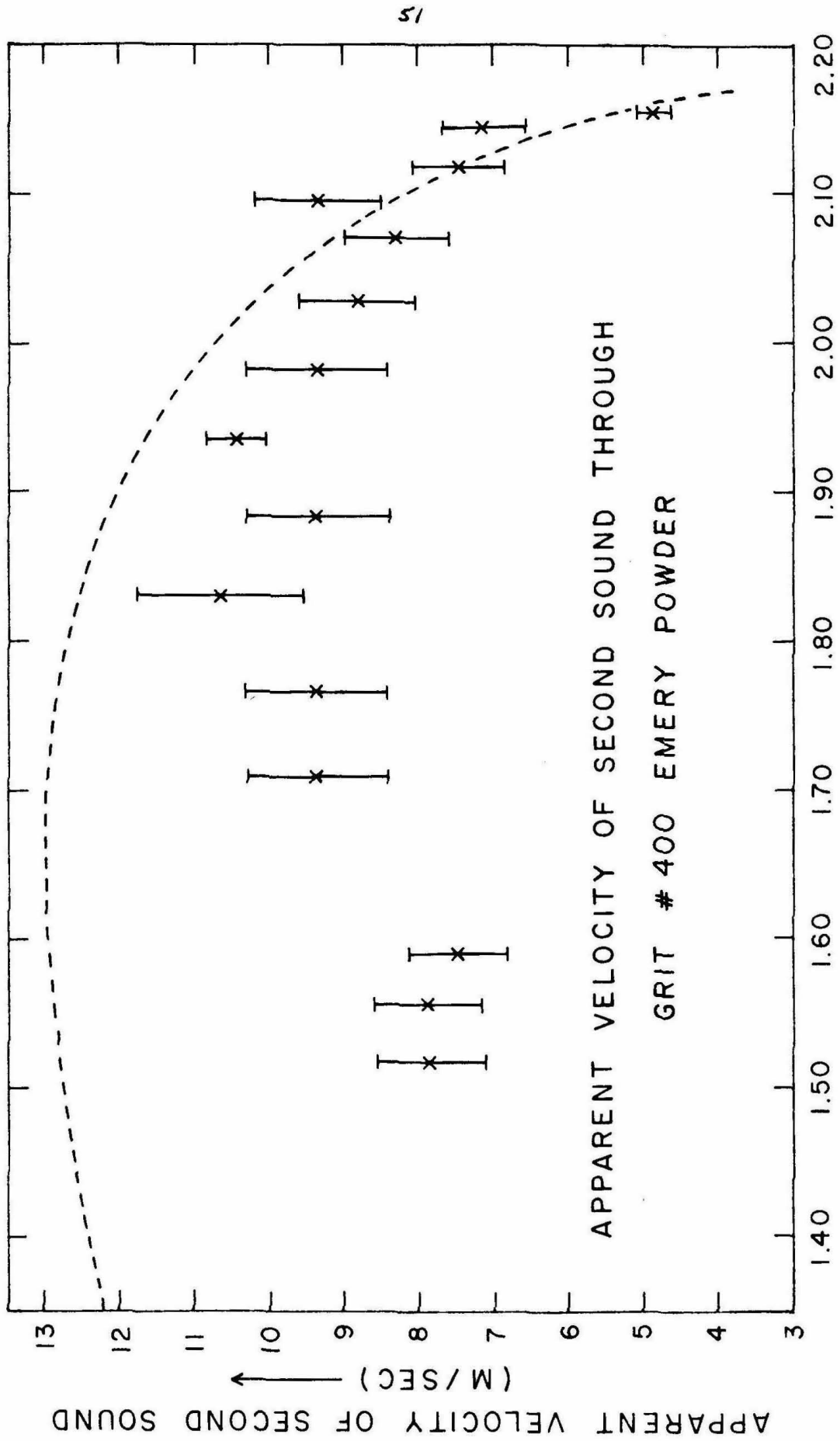


FIG. 7 TEMPERATURE (T) (°K)

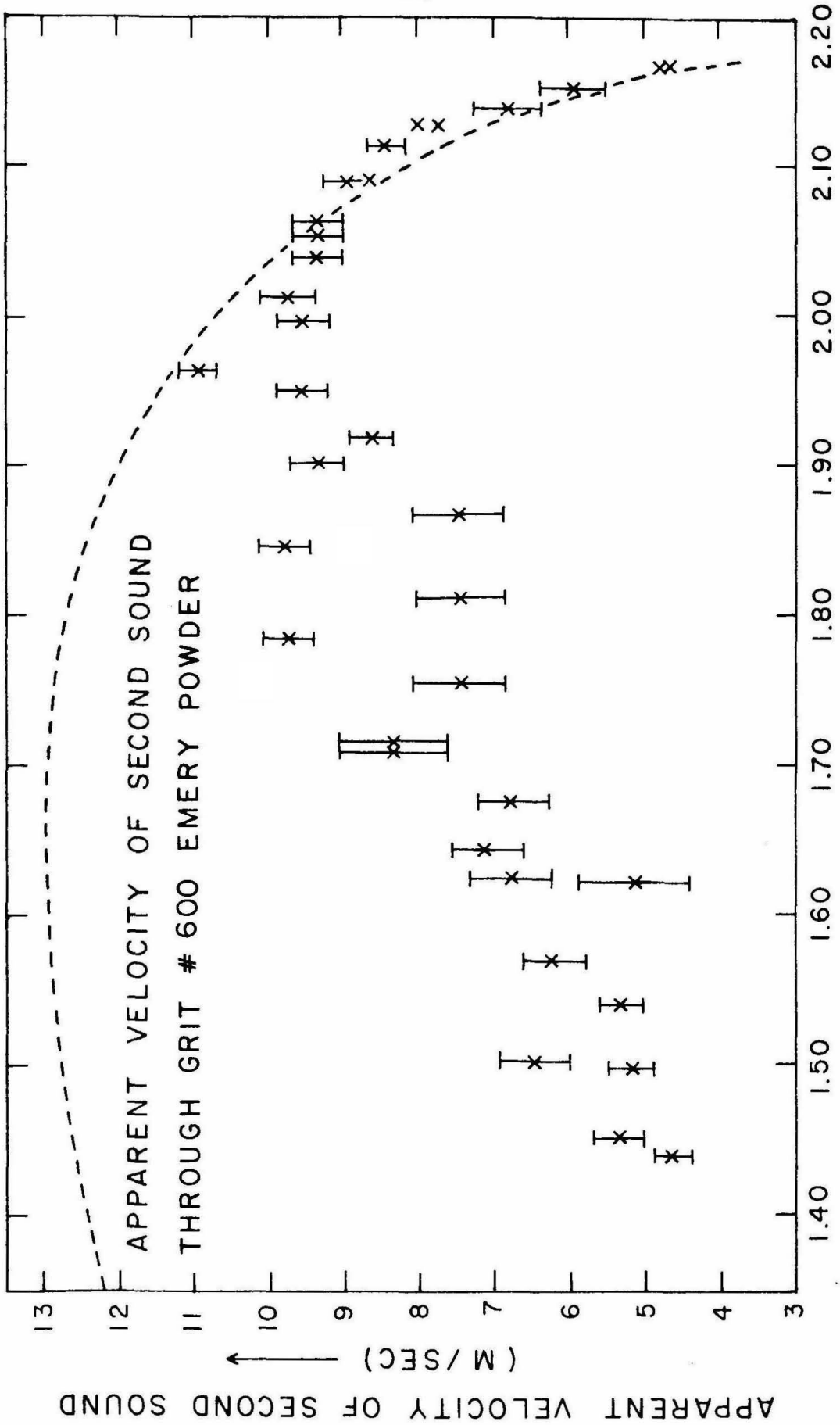


FIG. 8 TEMPERATURE (T) (°K)

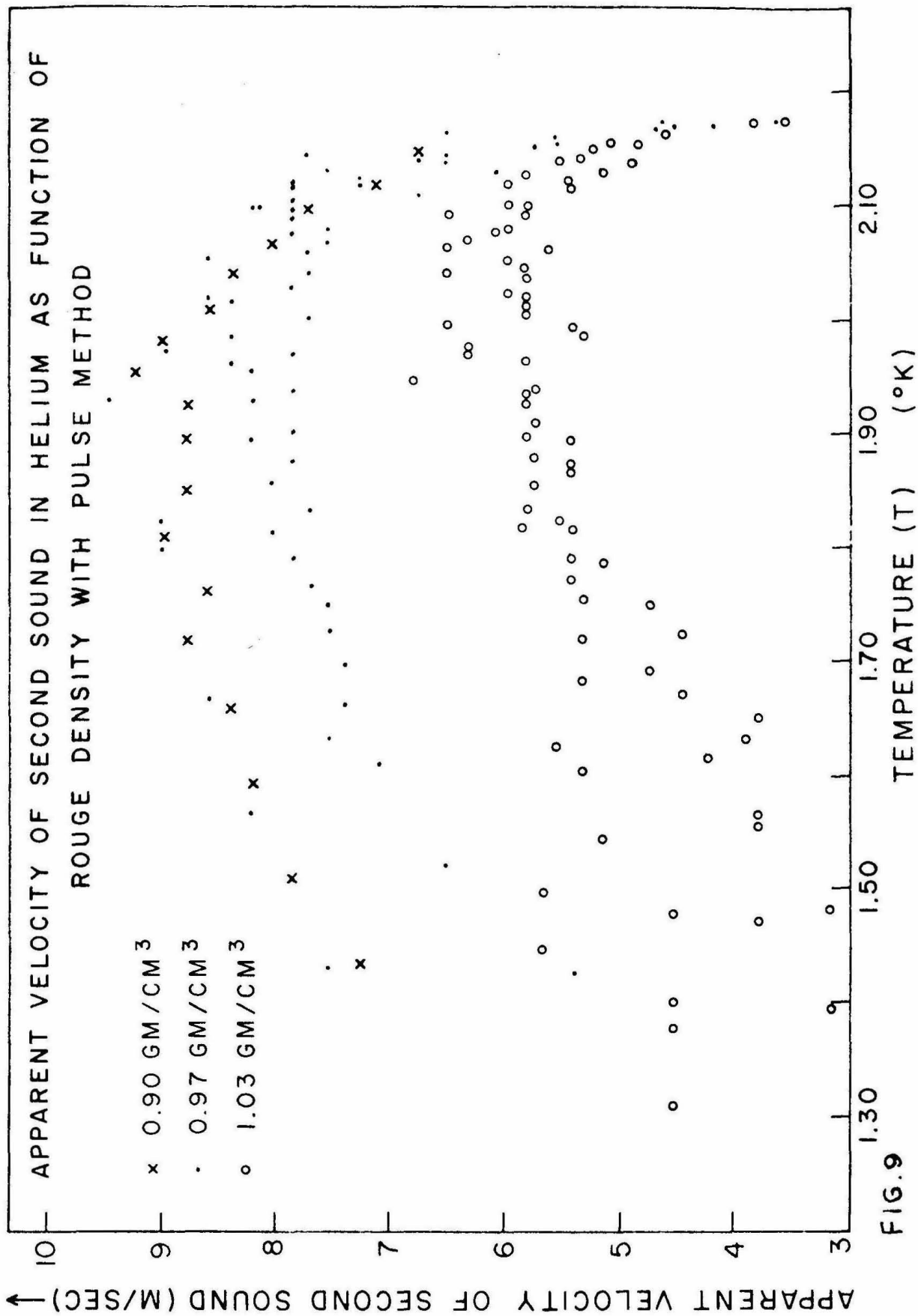


FIG. 9

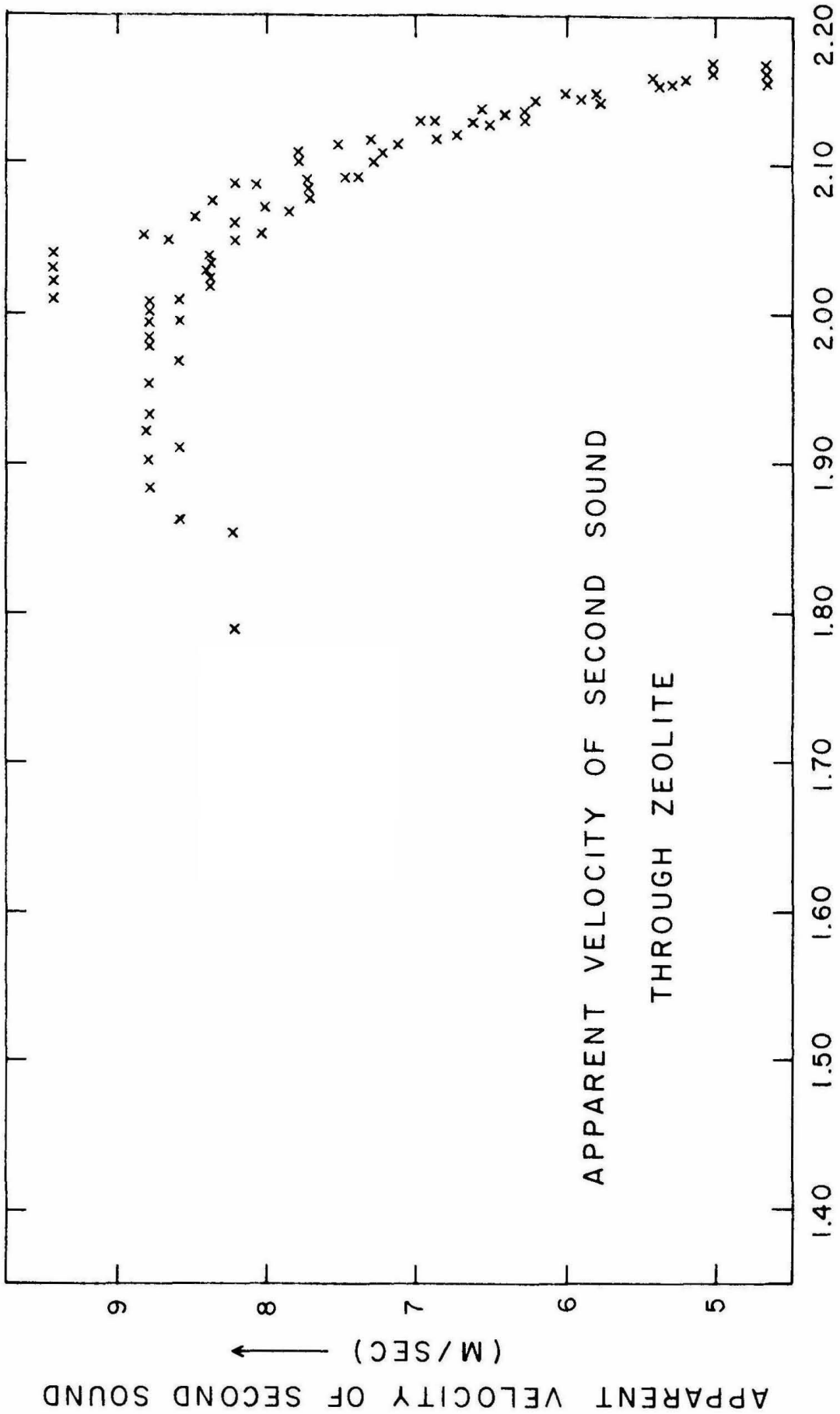


FIG. 10

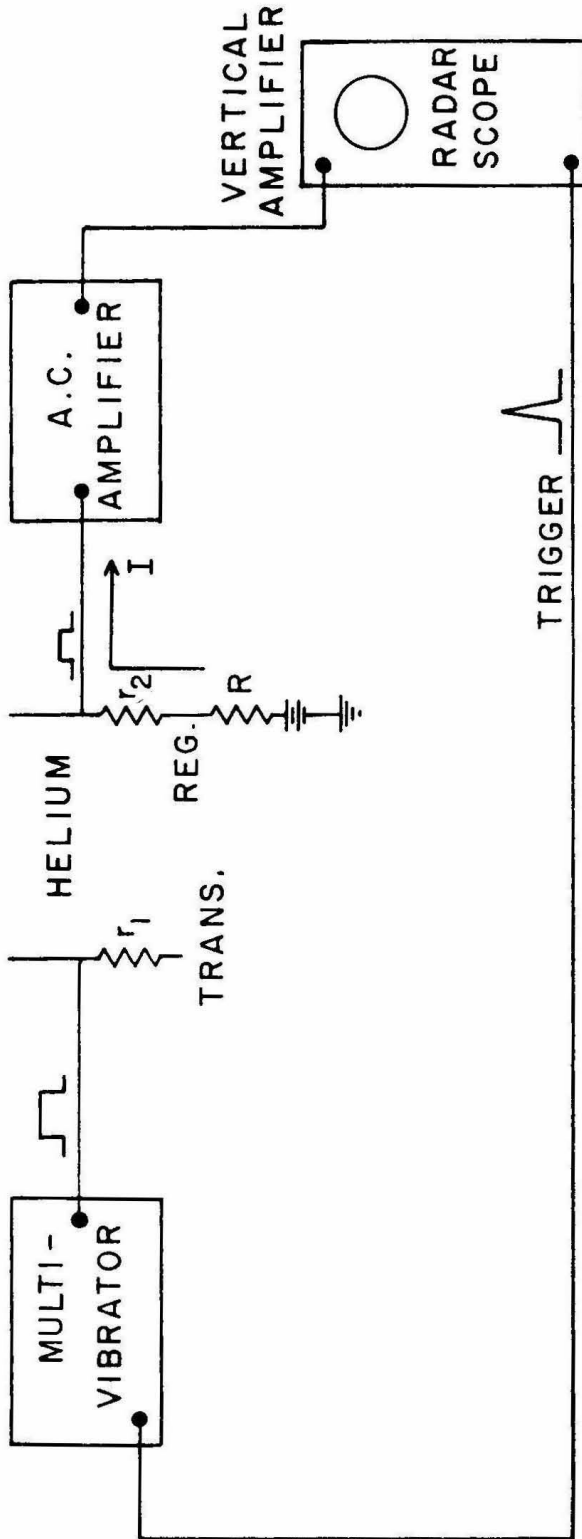


FIG. II SCHEMATIC OF ELECTRONIC SYSTEM
FOR PULSE METHOD

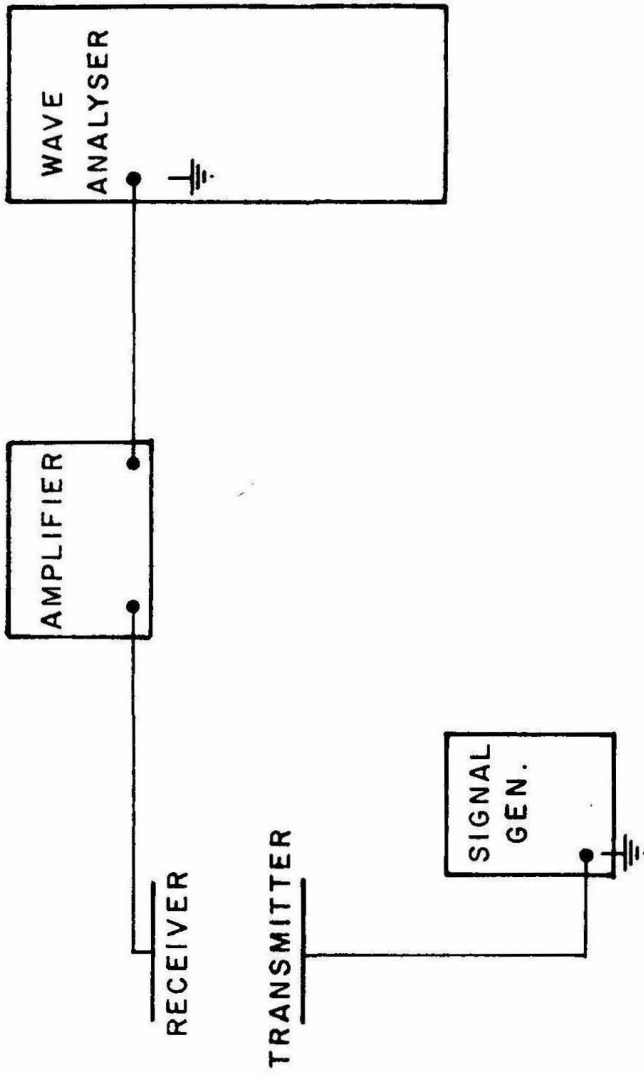


FIG. 12 SCHEMATIC OF ELECTRONIC SYSTEM FOR
STANDING WAVE METHOD

FIG. 13A TYPICAL RECEIVER OR TRANSMITTER
ELEMENT

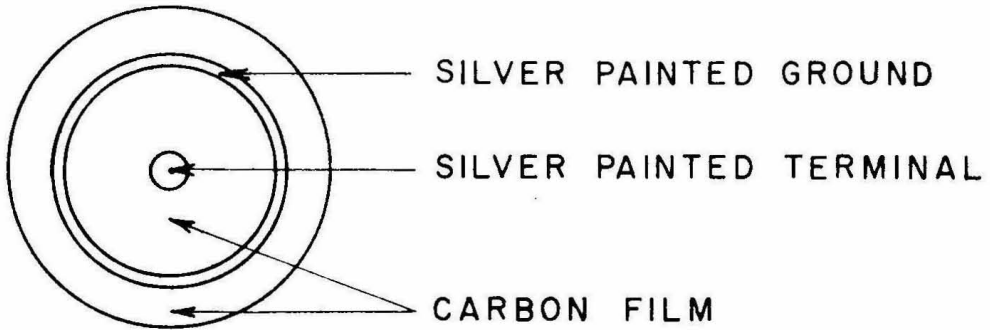
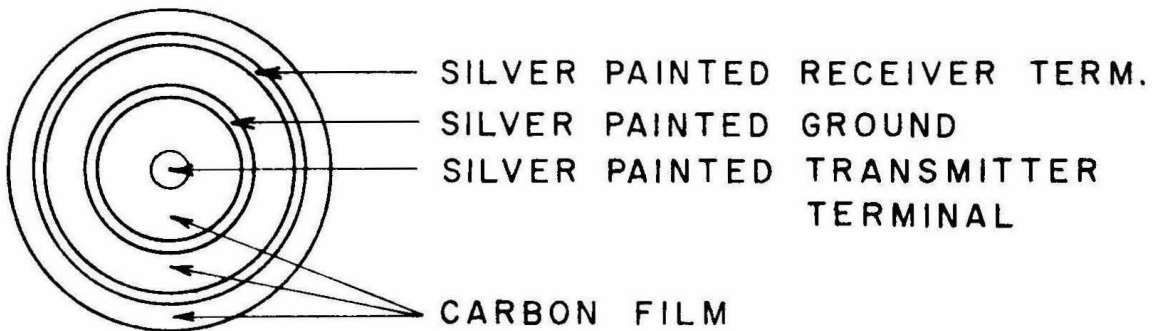
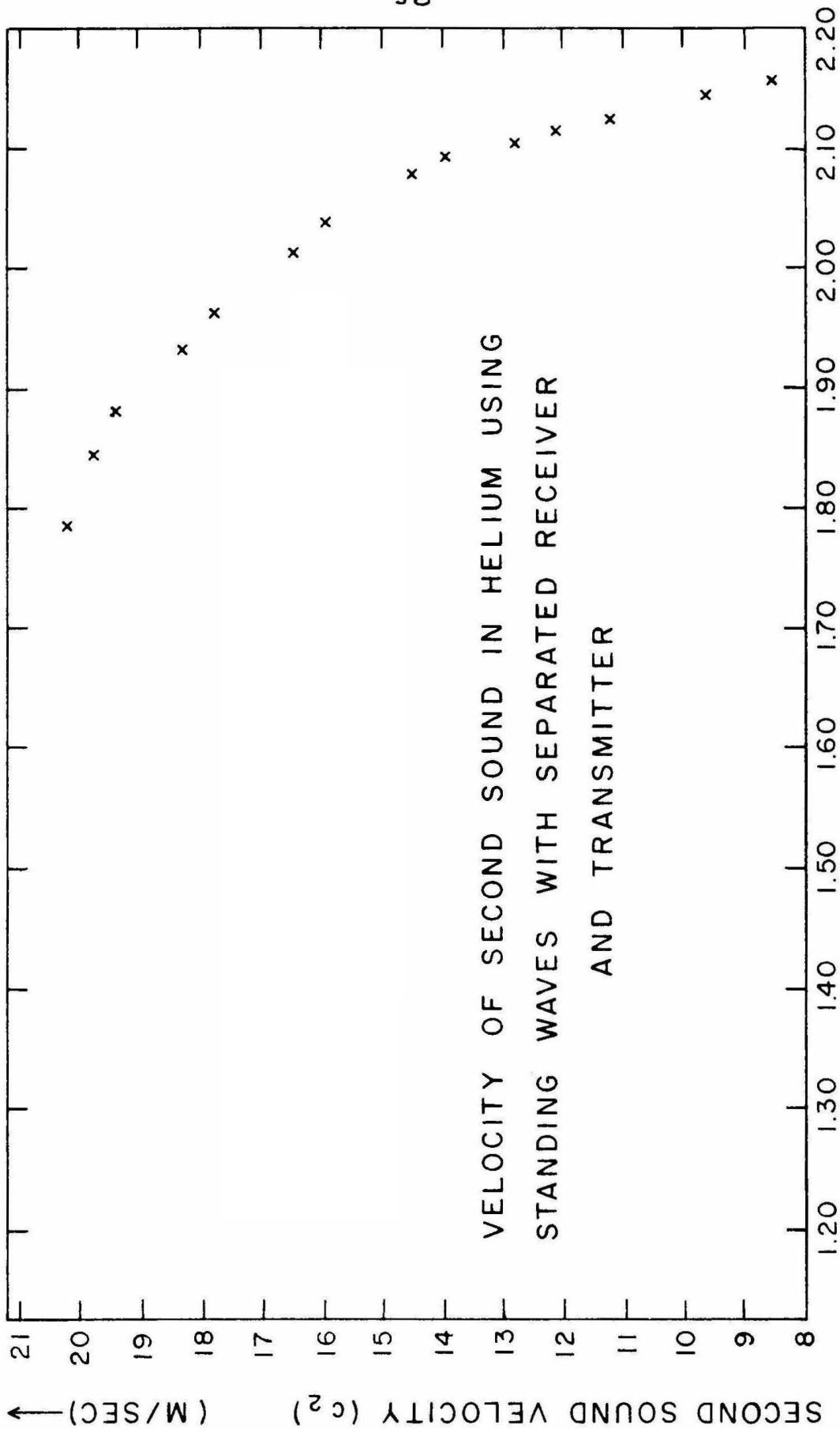


FIG. 13B TYPICAL COMBINED RECEIVER AND
TRANSMITTER ELEMENT





VELOCITY OF SECOND SOUND IN HELIUM USING
STANDING WAVES WITH SEPARATED RECEIVER
AND TRANSMITTER

FIG. 14.

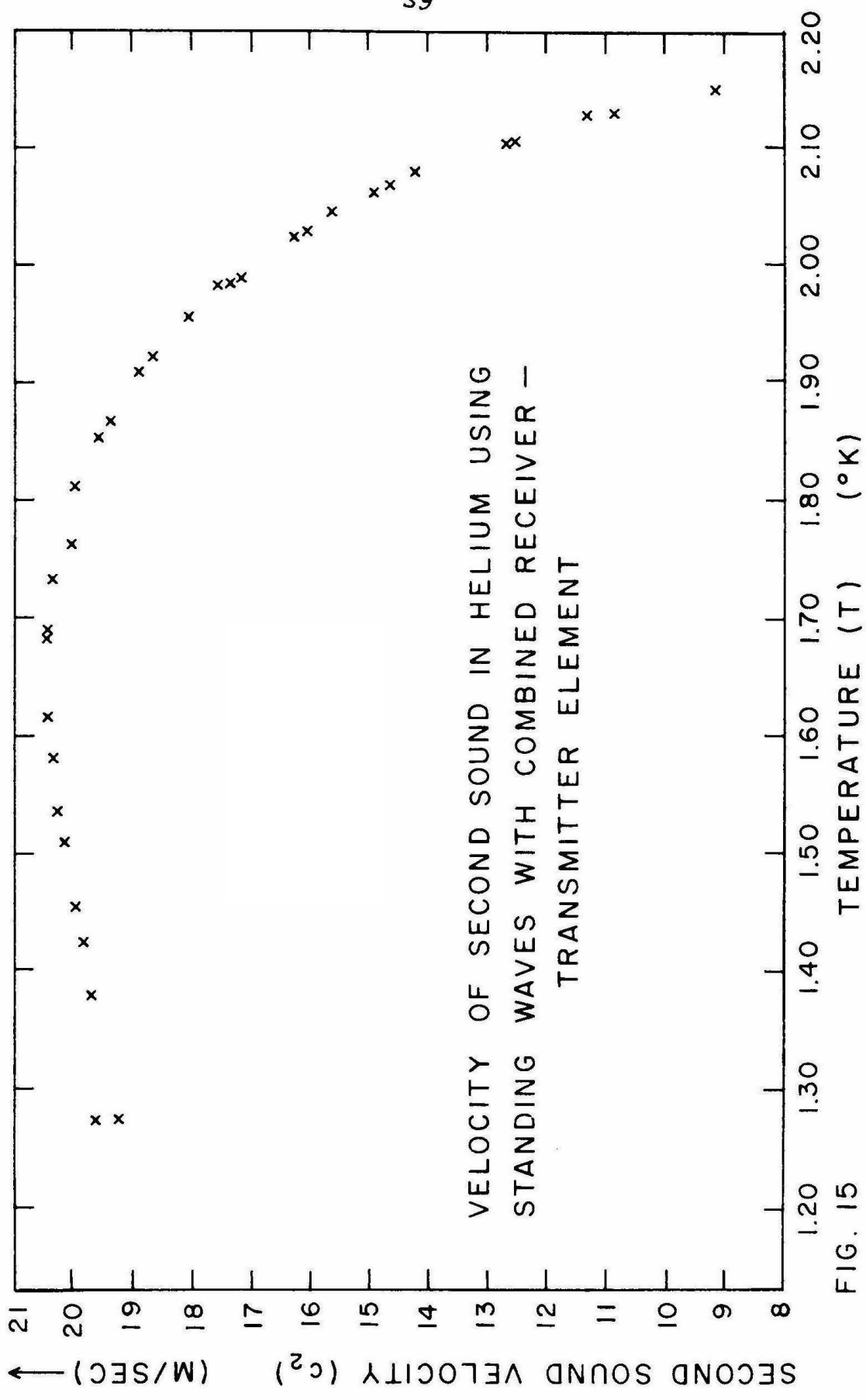
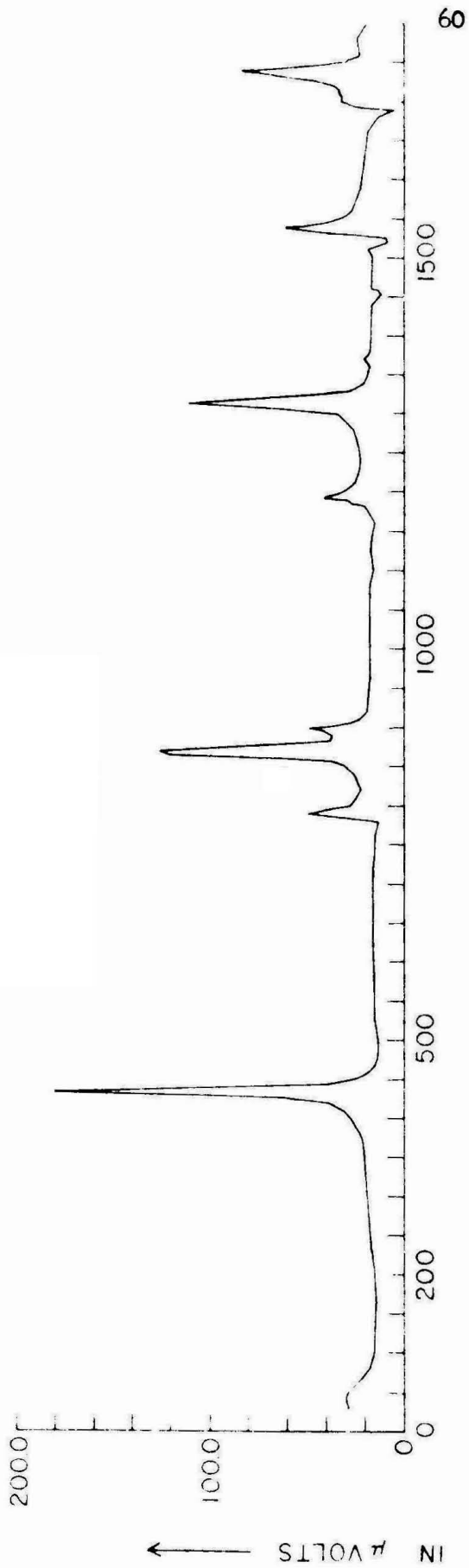


FIG. 15



SIGNALS RECEIVED IN μ VOLTS \leftarrow

SPECTRUM OF SIGNAL AS FUNCTION OF FREQUENCY OF SECOND SOUND
FOR CONTAINER 16.0 % FILLED WITH ROUGH 1.292°K

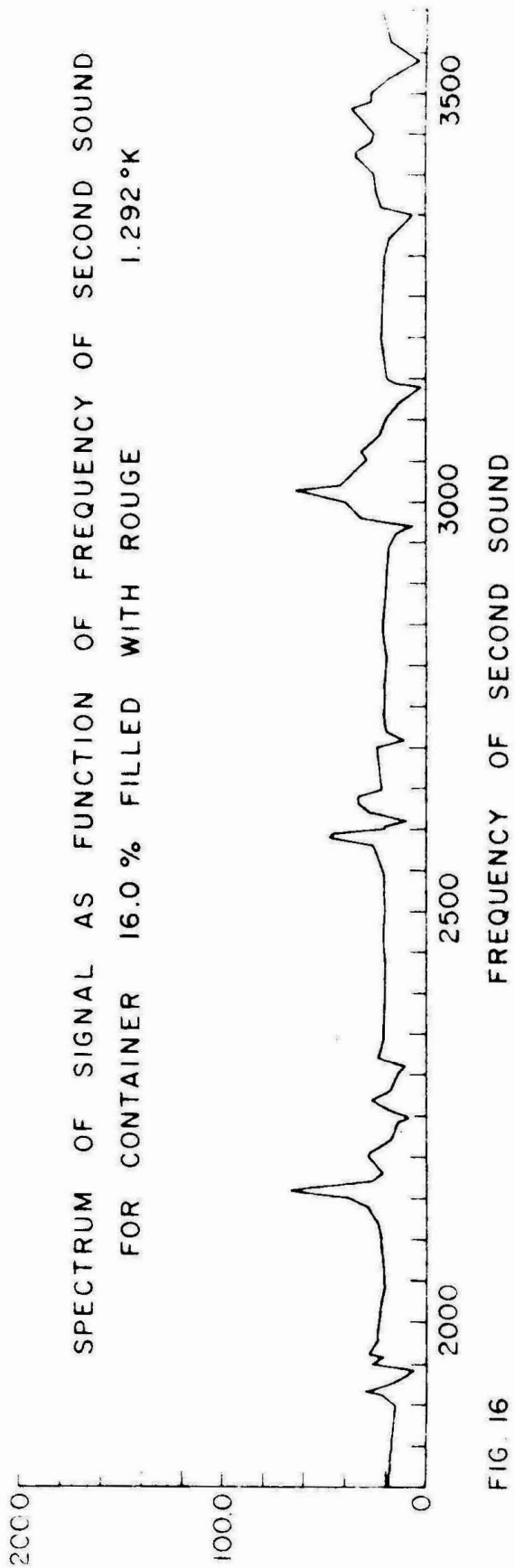
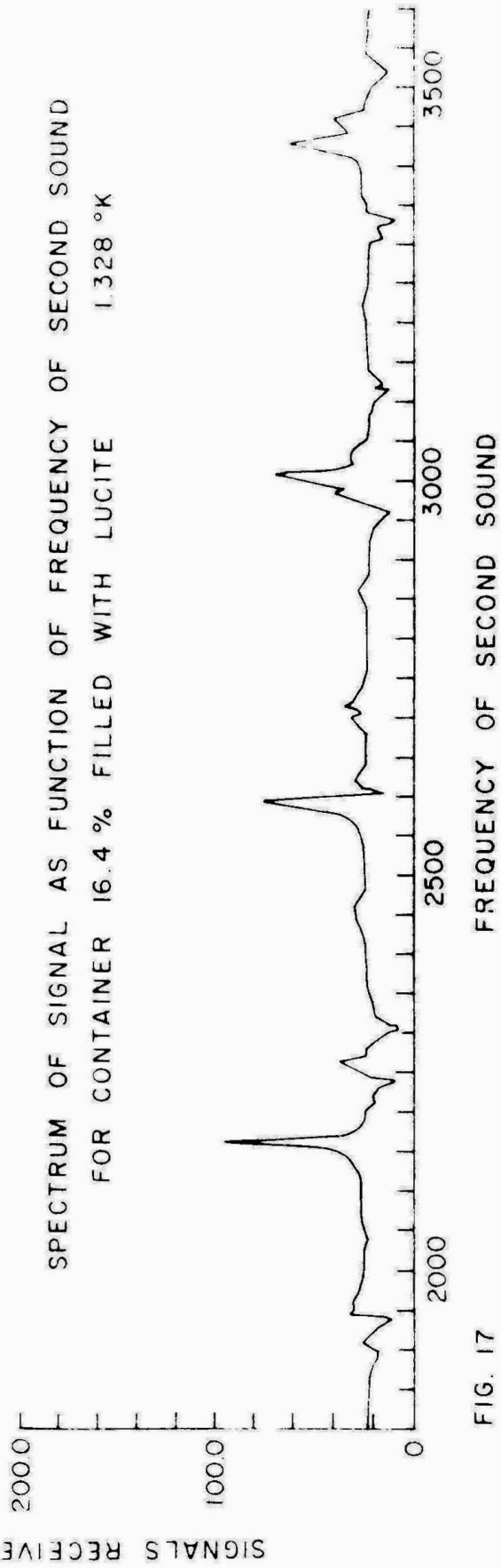
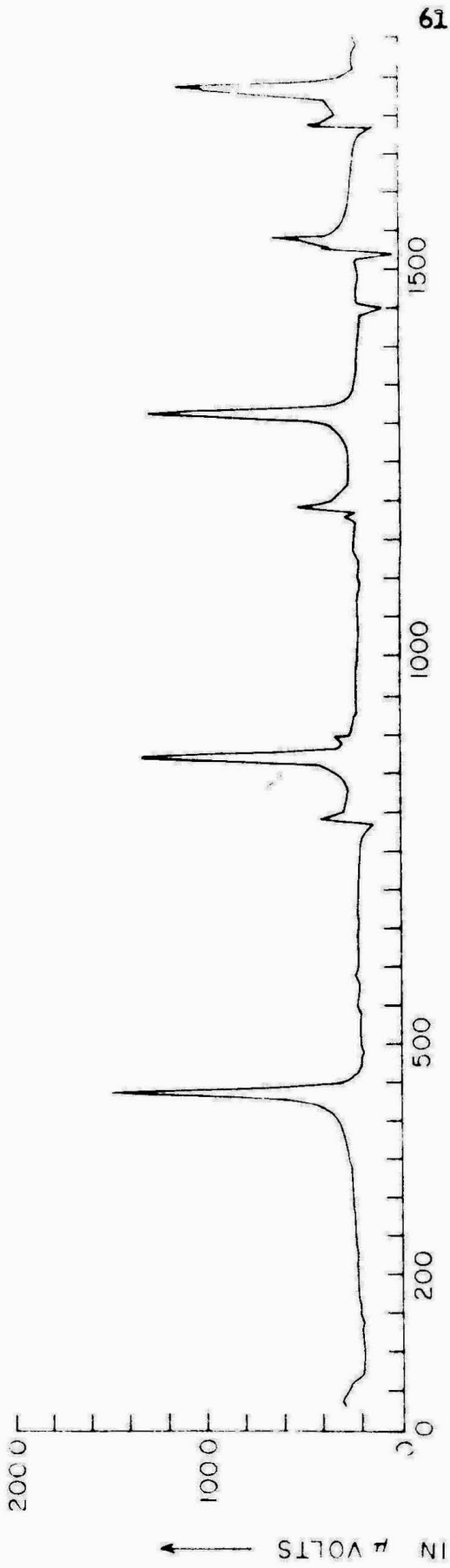


FIG. 16



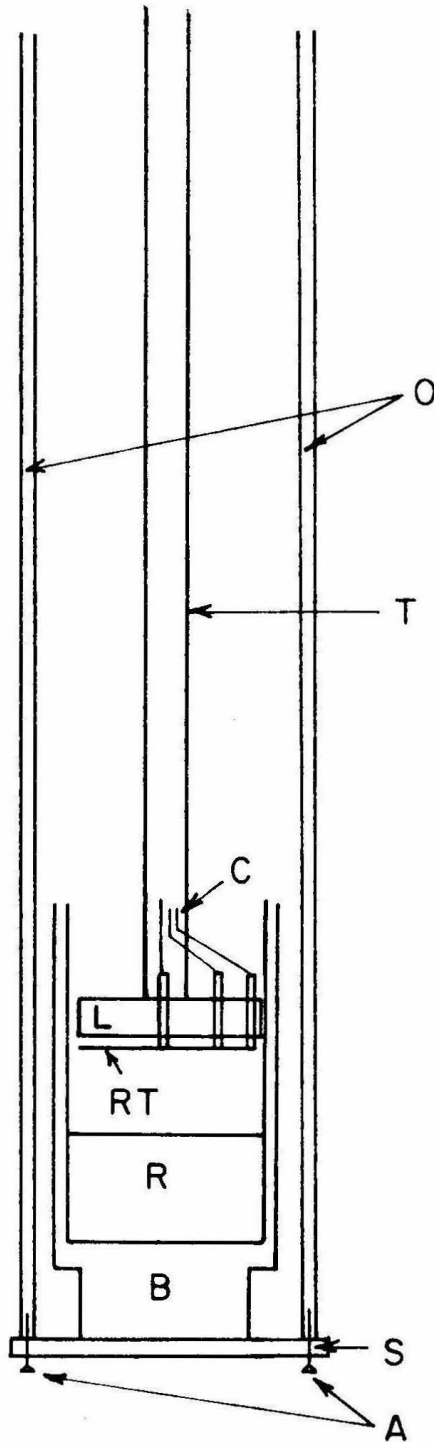
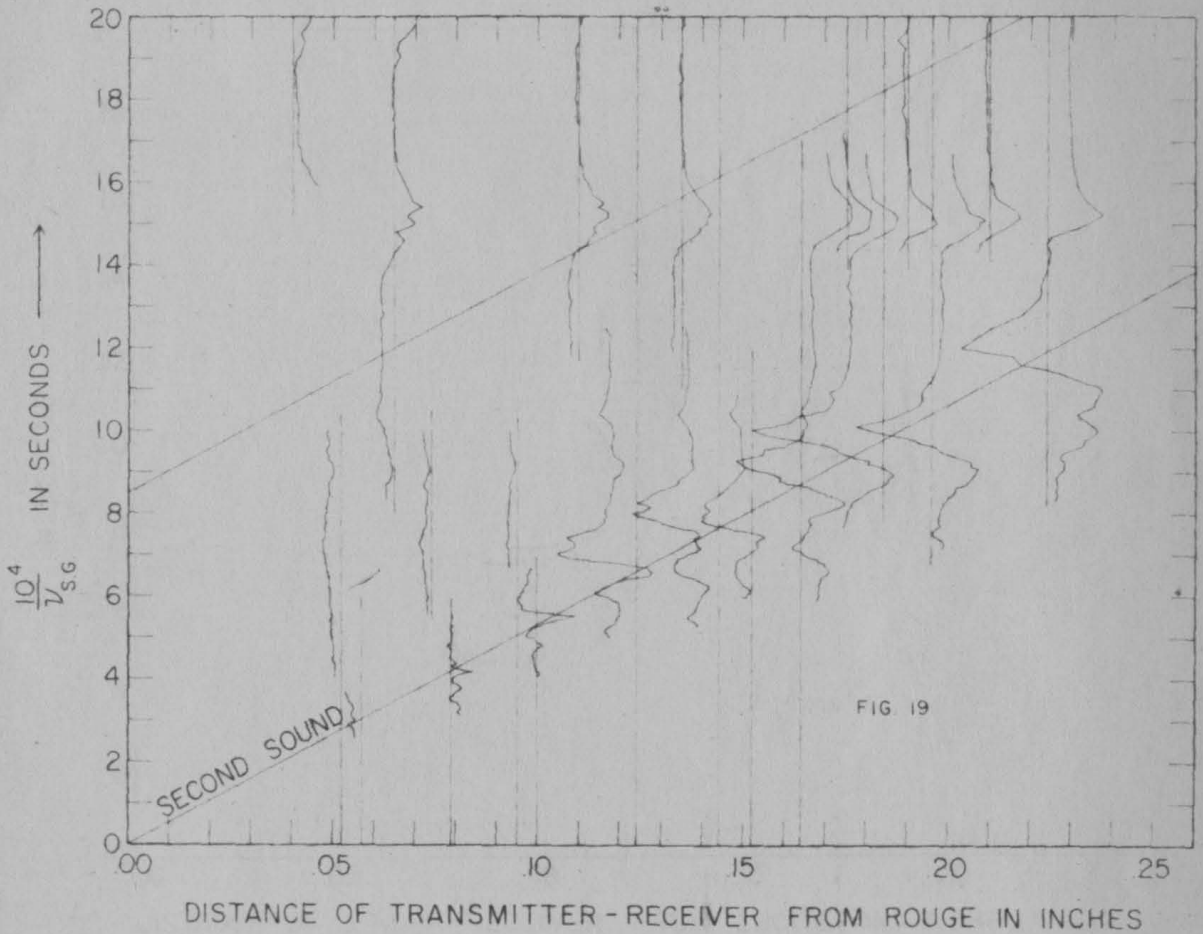
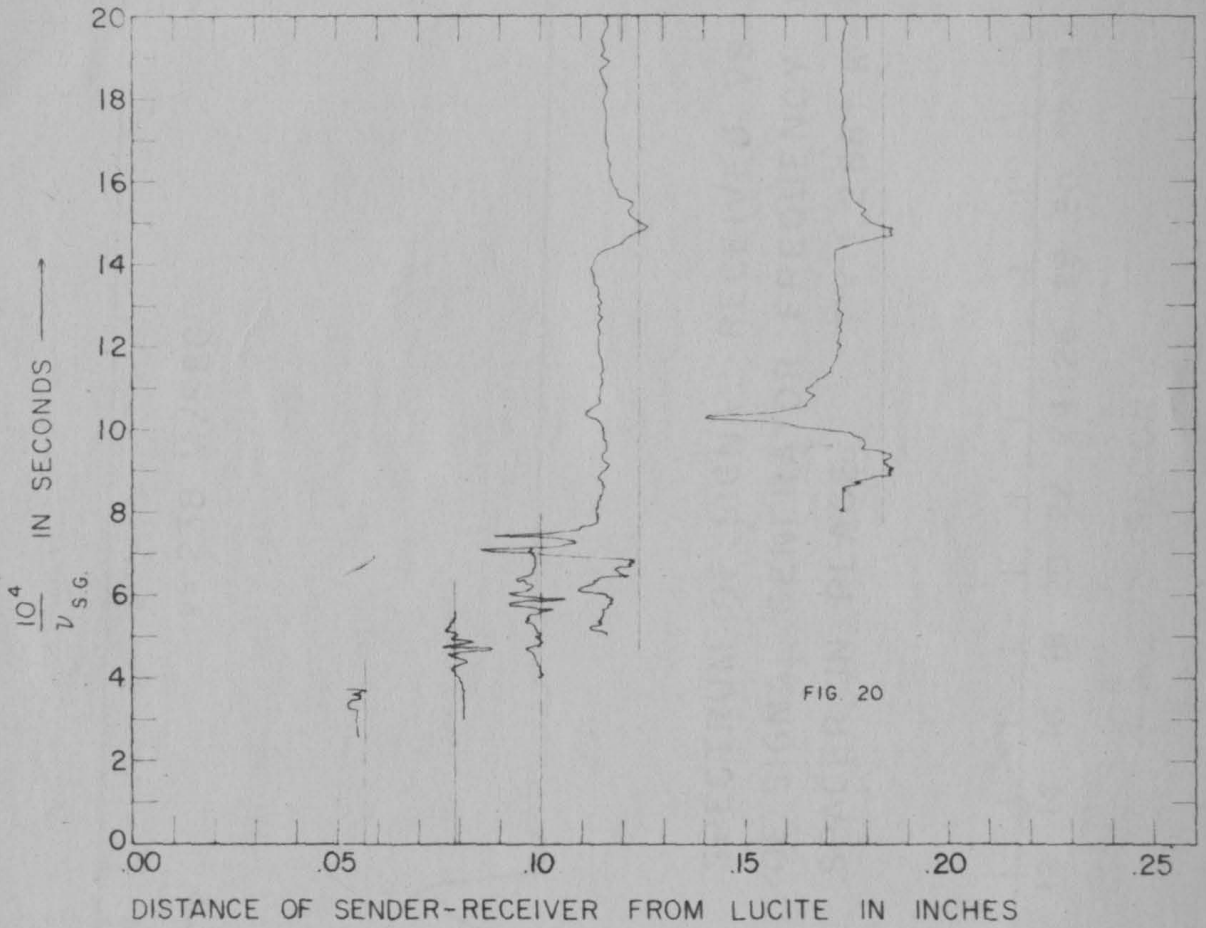


FIG.18 CONSTRUCTION DETAIL OF THE RESONANT
CHAMBER WITH VARIABLE HEIGHT



SPECTRUM OF SIGNAL HEIGHT AS FUNCTION OF
 RECIPROCAL OF SIGNAL GENERATOR
 FREQUENCY ALL MEASURED AT SEVERAL
 CHAMBER HEIGHTS WITH ROUGE BOTTOM.
 ROUGE DEPTH = 5.16 cm.
 T = 1.296 degrees K.



SPECTRUM OF SIGNAL HEIGHT AS FUNCTION OF
 RECIPROCAL OF SIGNAL GENERATOR
 FREQUENCY ALL MEASURED AT SEVERAL
 CHAMBER HEIGHTS WITH LUCITE BOTTOM.
 $T = 1.337$ degrees K.

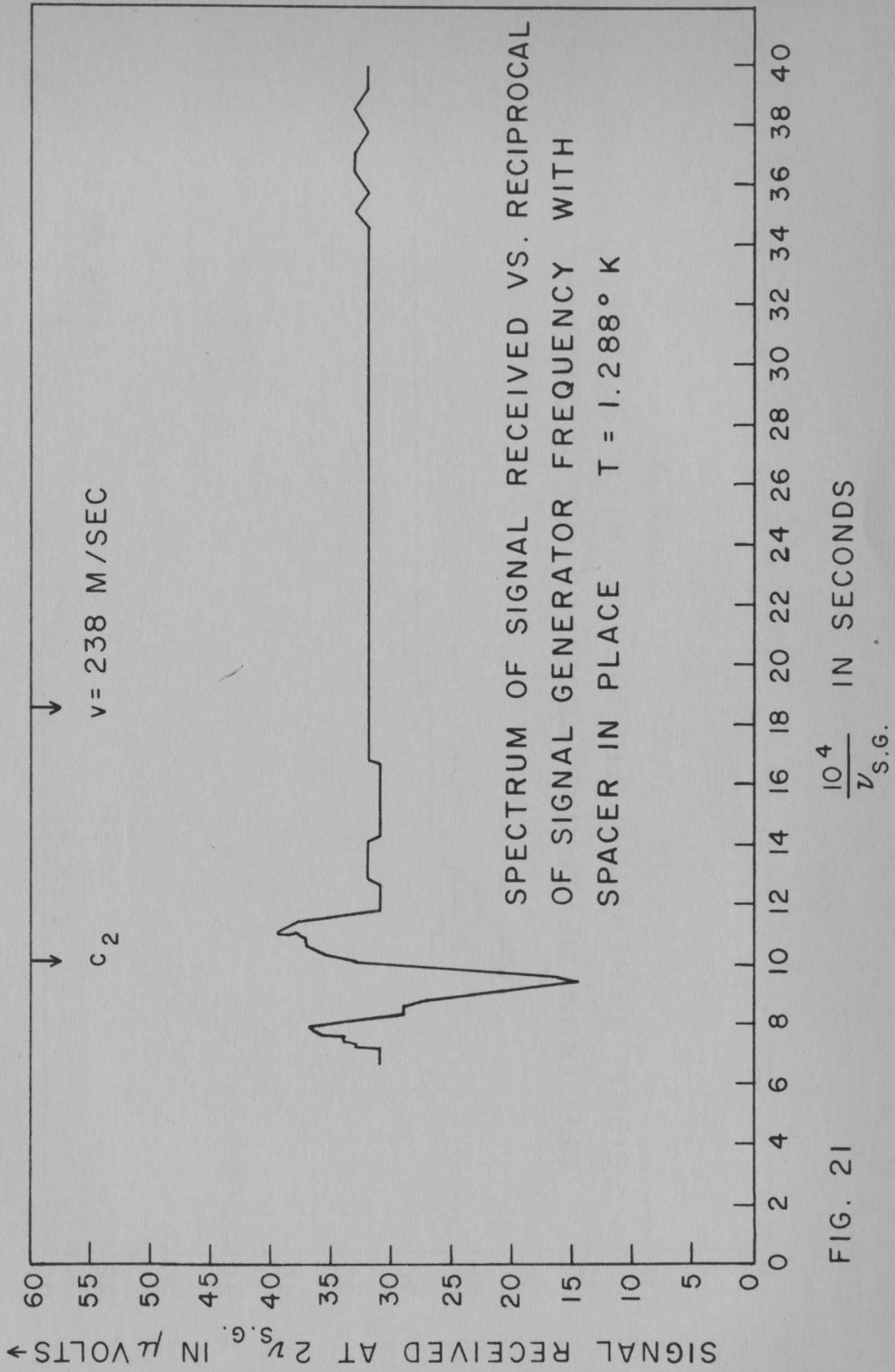


FIG. 21

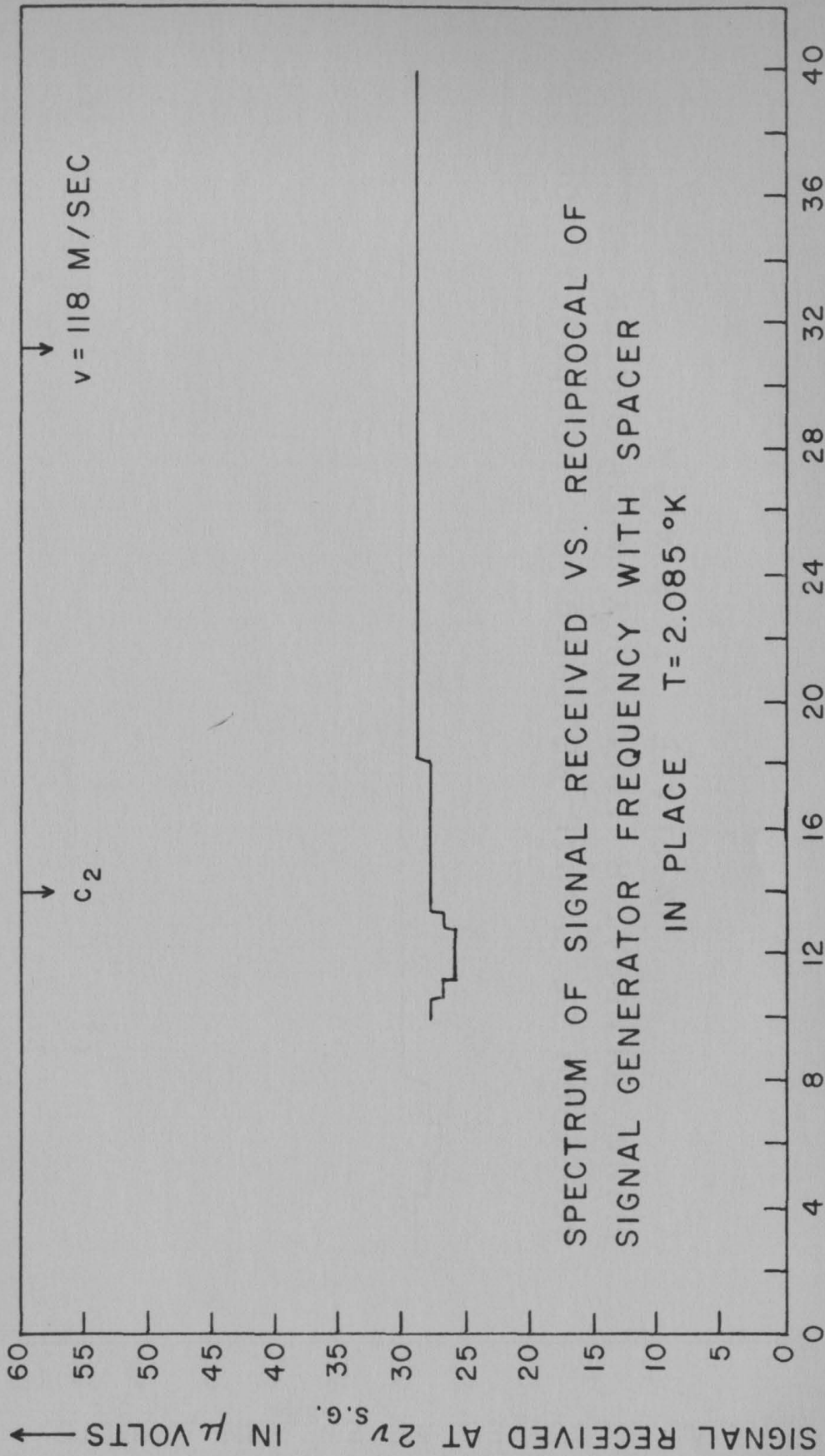


FIG. 22

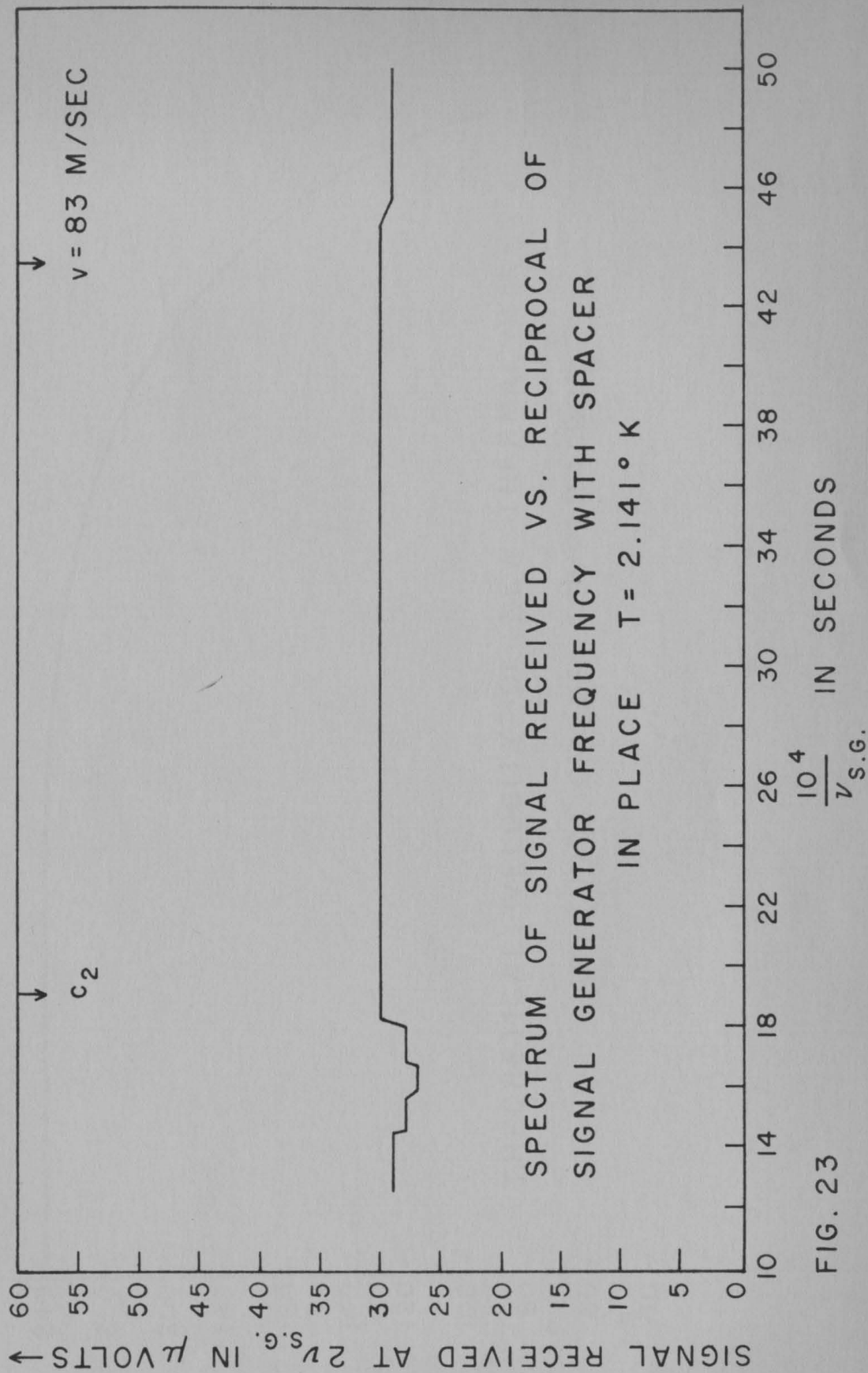


FIG. 23

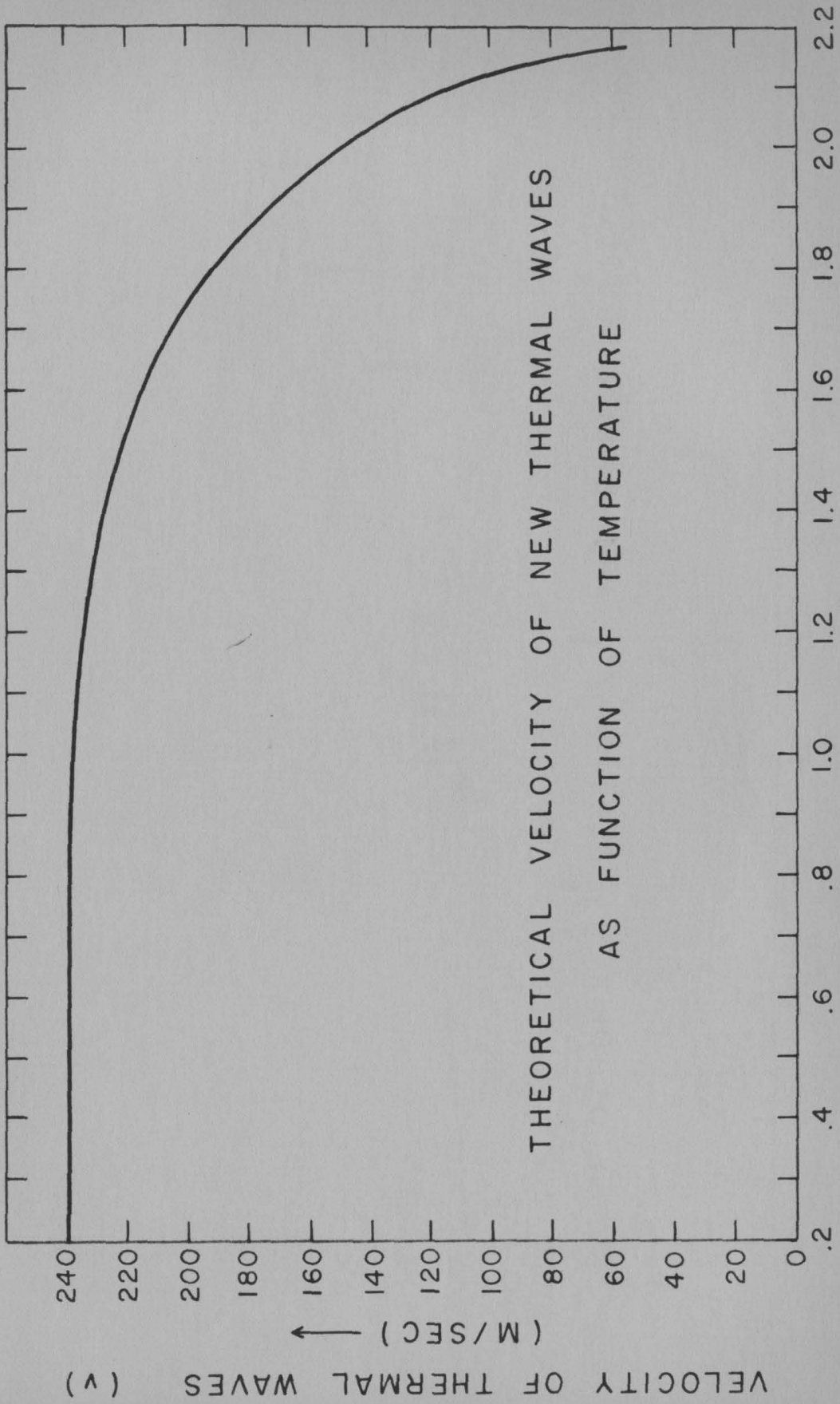
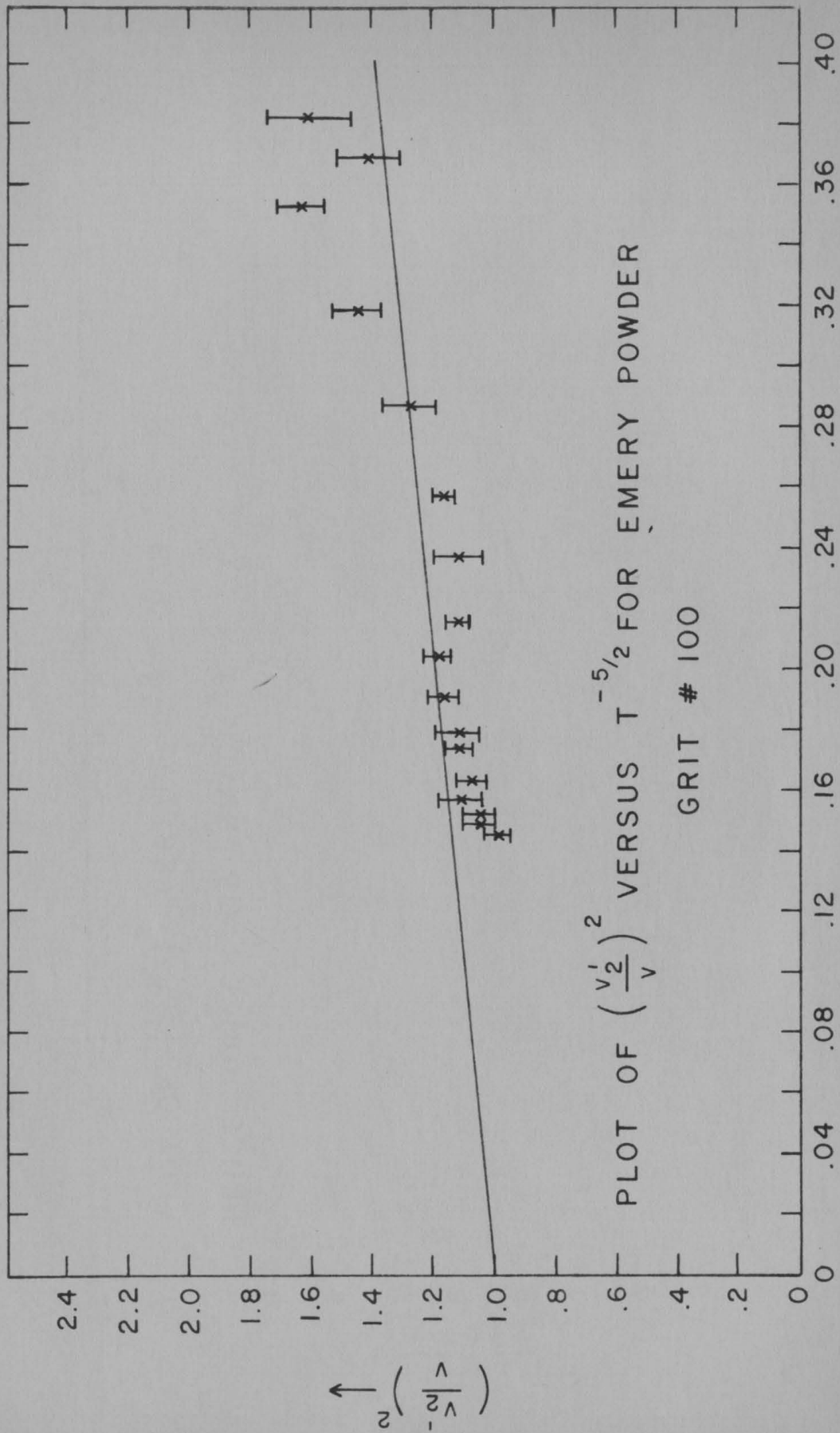


FIG. 24



$T^{-5/2}$

FIG. 25

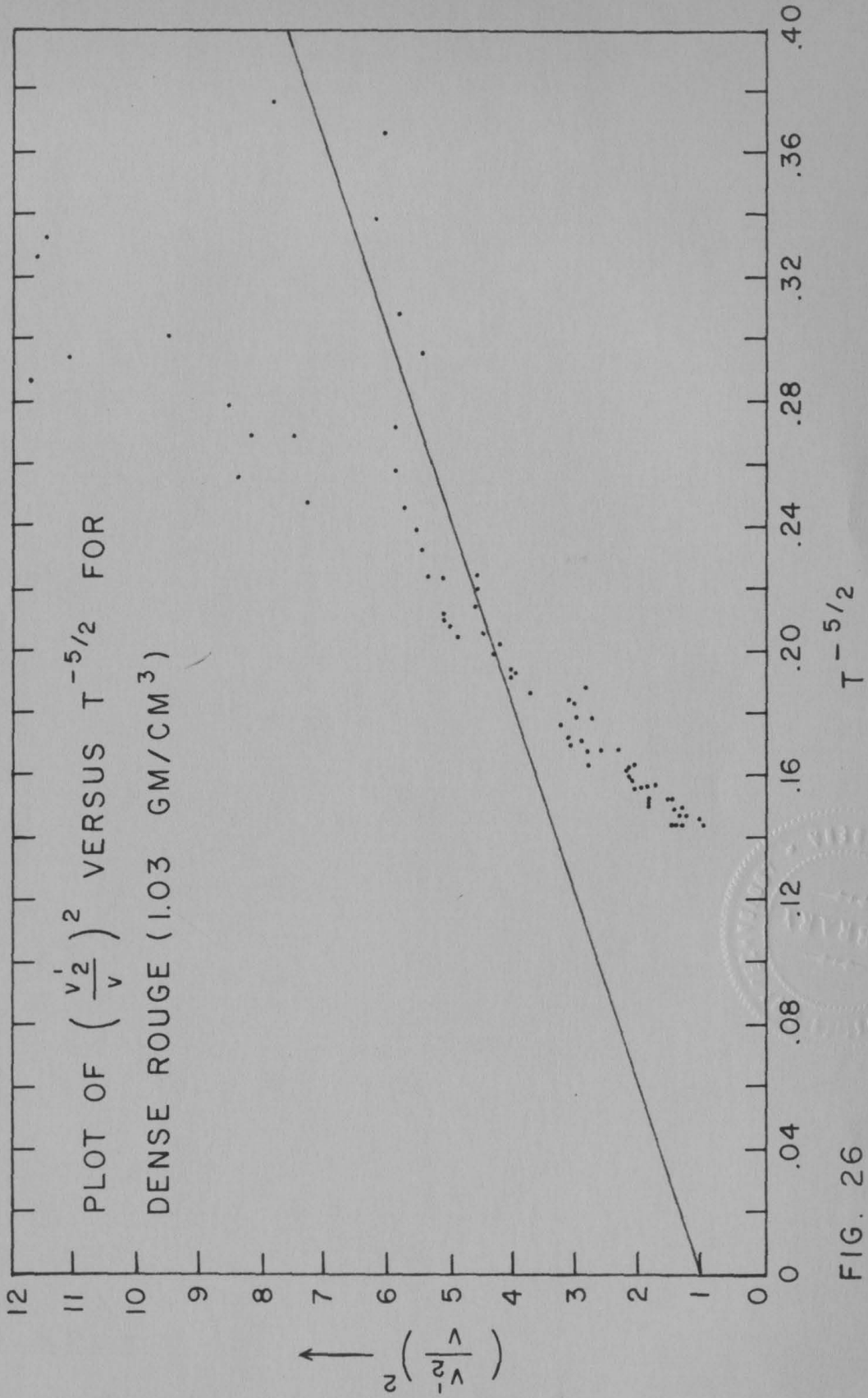


FIG. 26